Pedersen, R.B., Christie, D.M., and Miller, D.J. (Eds.)
*Proceedings of the Ocean Drilling Program, Scientific Results* Volume 187

# 7. Magnetic Properties of Mid-Ocean-Ridge Basalts from Ocean Drilling Program Leg 187[1]

Yen-Hong Shau,[2] Masayuki Torii,[3] Chorng-Shern Horng,[4] and Wen-Tzong Liang[4]

## ABSTRACT

The core samples of mid-ocean-ridge basalts (including Indian and Pacific type) recovered from the Southeast Indian Ridge (SEIR) area near the Australian Antarctic Discordance during Ocean Drilling Program Leg 187 were studied using rock magnetism, mineralogy, and petrography methods. On the basis of thermomagnetic analyses and low-temperature magnetometry, the dominant magnetic carrier in most of the basalt samples (pillow basalts) is characterized as titanomaghemite, which presumably formed by low-temperature oxidation of primary titanomagnetite. Some samples from unaltered massive basalts contain nearly unoxidized titanomagnetite as the main magnetic mineral. A metadiabase sample showing greenschist facies metamorphism contains magnetic minerals dominated by magnetite. The pillow basalts contain titanomaghemite ranging from stable single-domain to pseudo-single-domain (PSD) grains, and the majority are characterized by a single stable component of remanence. The massive basalts show hysteresis features of larger PSD grains and contain a very low coercivity remanence. The values of natural remanent magnetization (NRM) of the samples in this SEIR area are on the same order as those of other oceanic ridge basalts. They show a general decreasing trend of NRM with increasing crust age. However, the values of NRM show no correlation either with the tectonic zonations (Zone A vs. Zone B) or with the mantle provinces (Pacific vs. Indian types).

[1]Shau, Y.-H., Torii, M., Horng, C.-S., and Liang, W.-T., 2004. Magnetic properties of mid-ocean-ridge basalts from Ocean Drilling Program Leg 187. *In* Pedersen, R.B., Christie, D.M., and Miller, D.J. (Eds.), *Proc. ODP, Sci. Results,* 187, 1–25 [Online]. Available from World Wide Web: <http://www-odp.tamu.edu/publications/187_SR/VOLUME/CHAPTERS/204.PDF>. [Cited YYYY-MM-DD]
[2]Department of Marine Resources, National Sun Yat-sen University, Kaohsiung 80424, Taiwan. **yhshau@mail.nsysu.edu.tw**
[3]Department of Biosphere-Geosphere System Science, Okayama University of Science, Okayama 700-0005, Japan.
[4]Institute of Earth Sciences, Academia Sinica, Taipei 11529, Taiwan.

Initial receipt: 1 May 2003
Acceptance: 8 September 2003
Web publication: 19 February 2004
Ms 187SR-204

## INTRODUCTION

Marine magnetic anomaly patterns record the history of global plate movements and variations in the Earth's magnetic field. Interpretation of those patterns 40 yr ago shed light on the theory of plate tectonics (Vine and Matthews, 1963) and is fundamental to understanding the evolution of oceanic crust. However, there have been questions and debates regarding the source layers of the marine magnetic anomalies and the magnetization of oceanic crust with respect to the change of time and space (e.g., Dunlop and Özdemir, 1997; Johnson and Tivey, 1998). For example, what is the thickness and nature of the magnetic source layer that contributes to the marine magnetic anomalies? Is there a significant time lag for the magnetization of oceanic crust after their formation at the spreading centers (e.g., Hall and Muzzatti, 1999; Shau et al., 2000)? How and why does the natural remanent magnetization (NRM) of the oceanic crust vary with respect to the age and depth of the crust (e.g., Johnson and Pariso, 1993)? What is the exact magnetization process of the oceanic crust? Is the contribution of NRM of the crust mainly from thermoremanent magnetization (TRM) acquired during subsolidus cooling or from chemical remanent magnetization (CRM) formed as a result of alteration? In order to understand these fundamental questions concerning the marine magnetic anomalies, we first need to know the nature and origin of main magnetic carriers in the oceanic crust, including mineral type, composition, grain size, texture, mineral paragenesis, and their magnetic properties. On the basis of our knowledge of the magnetic minerals in oceanic crust, it is then possible to solve the debates and to answer the above questions.

In the present study, we combined rock magnetism, mineralogy, and petrography methods to study magnetic minerals in the core samples from Ocean Drilling Program (ODP) Leg 187. The study aimed to (1) present magnetic properties of basaltic samples from the Southeast Indian Ridge (SEIR) area and correlate the whole-rock magnetic properties with petrographic features of magnetic minerals, (2) characterize the nature and formation mechanism of magnetic minerals in the oceanic-ridge basalts, and (3) study variations of magnetic properties and related magnetic minerals with crust age.

## GEOLOGICAL SETTING AND SAMPLE DESCRIPTIONS

During Leg 187, 23 holes were drilled at 13 sites (Sites 1152–1164) to recover mid-ocean-ridge basalt (MORB) in the Southeast Indian Ocean between Australia and Antarctica (Fig. F1). The 13 drill sites are located on 14- to 28-Ma seafloor within the area of 126°–135°E and 41°–46°S, which is ~400 km north of the SEIR and on the eastern boundary of the Australian Antarctic Discordance (AAD). The AAD is a segment of the SEIR between 120° and 128°E that is characterized by anomalously deep bathymetry, low gravity, and rugged seafloor topography (Weissel and Hayes, 1971; Hayes and Conolly, 1972). By using contrasts in these physical and morphologic properties, Weissel and Hayes (1971) classified the SEIR into three longitudinal zones, A, B, and C, from east to west; Zone B incorporates the AAD. The eastern boundary of the AAD is an approximately north-south–tracing fracture zone that separates Zone A, with smooth off-axis topography to the east, from Zone B, with

F1. Locations of Leg 187 drill sites, p. 12.

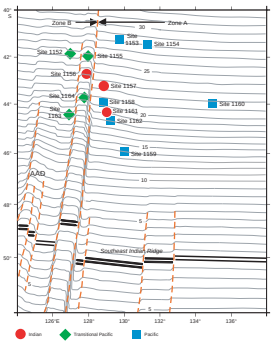

rough off-axis topography to the west. Geochemical analyses of dredge samples from the SEIR reveal that the eastern border of AAD is indeed a remarkable isotopic boundary between "Pacific-type" and "Indian-type" upper-mantle provinces (e.g., Klein et al., 1988; Pyle et al., 1992; Christie et al., 1998). Aeromagnetic data collected in this area show that the magnetic anomalies are of large amplitude east of the AAD (Zone A), low amplitude within the AAD (Zone B), and normal amplitude west of the AAD (Zone C) (e.g., Anderson et al., 1980; Vogt et al., 1984). It has been suggested that the high magnetic anomaly amplitudes found along the easternmost segment of the Southeast Indian Ridge (Zone A) are caused by the high NRMs of basalts, which are in turn caused by an increase of titanomagnetite concentration in the Zone A basalts (Anderson et al., 1980).

The purpose of Leg 187 was to locate the boundary between Indian and Pacific mantle provinces in the off-axis area. On the basis of the geochemical data obtained from the recovered MORB samples, each of the 23 holes was assigned to the Indian, Pacific, or Transitional-Pacific upper mantle type (Shipboard Scientific Party, 2001) (Fig. **F1**). Detailed descriptions including objectives, shipboard analyses, and achievements of Leg 187 can be found in the Leg 187 *Initial Reports* volume (Christie, Pedersen, Miller, et al., 2001).

A total of 94 slab samples, each measuring ~5 cm (length) × 4 cm (width) × 1 cm (height), were collected from the recovered cores for the present study. Most of the samples are pillow basalts, either aphyric or phyric, with sparsely to moderately distributed phenocrysts of plagioclase, clinopyroxene, or olivine. Plagioclase is the most abundant phenocryst in the phyric basalts. A few samples are basalt rubble or basaltic breccia. Three massive basalt samples from Hole 1160B (Samples 187-1160B-4R-1, 72–77 cm [#63], 7R-1, 59–62 cm [#65], and 9R-1, 111–116 cm [#67]) are intercalated with pillow basalt samples. A metadiabase sample from Hole 1162A (Sample 187-1162A-5R-1, 33–37 cm [#74]) shows greenschist facies metamorphism. Most samples have been subjected to alteration and are lighter bluish gray or brownish rather than dark gray or black, like fresh basalts. The pillow basalt samples show curved or convex outlines and generally have a light-colored core embraced by a darker outer zone (~0.5- to 1-cm-wide rim zone) on the cutting sections. For detailed studies, we further sampled the rim zone and core zone from many basalt specimens; a total of 114 specimens were obtained. Samples used for magnetic measurements were taken ~0.5 cm from pillow margins for the rim zone samples and ~1–3 cm from pillow margins for the core zone samples. The identification numbers and the attributed mantle provinces (Shipboard Scientific Party, 2001, table T2) of all the collected samples are shown in Table **T1.**

**T1.** Magnetic properties of the cored samples, p. 22.

## ANALYTICAL TECHNIQUES

Slab samples were cut in two for preparing polished thin sections and for rock magnetic measurements. We prepared 114 cubic specimens, 0.7–1 cm long, for paleomagnetic measurements of NRM and magnetic susceptibility. These 1- to 3-g specimens were constrained in 1-in Teflon cylinders and fixed with nonmagnetic screws during measurement. NRM intensities were measured with a Natsuhara Giken SMD-88 spinner magnetometer. Values of low-field magnetic susceptibility ($k$; volume specific) were measured with a Bartington Instruments MS2 system. Volume and density of each specimen were determined in order

to calculate volume-specific magnetic parameters. In order to examine the stability of the remanent magnetization, we carried out stepwise thermal demagnetization and alternating-field (AF) demagnetization of the NRM on 16 and 24 selected specimens, respectively. Thermal demagnetization was conducted with a Magnetic Measurements MMTD80 thermal demagnetizer. A total of 25 heating steps from room temperature to 580°C were employed (i.e., 25°, 80°, 120°, 160°, and increments of 20° from 160° to 580°C). After each heating step, a 2G Enterprises superconducting rock magnetometer measured remanent magnetization. For AF demagnetization, specimens were treated with a triaxial AF demagnetizer in-line with the cryogenic magnetometer. AF demagnetization was performed at 26–28 steps to 150 mT, with 5- to 10-mT increments between steps.

Crushed samples of 1–4 mg were used for measurements of magnetic hysteresis parameters including saturation magnetization ($M_s$), remanent saturation magnetization ($M_{rs}$), coercivity ($B_c$), and remanent coercivity ($B_{cr}$). We measured hysteresis parameters using a Princeton Measurements MicroMag 2900 alternating gradient force magnetometer with a maximum field of 1 T. $M_s$ and $B_c$ were determined after correcting the contribution of the paramagnetic component by applying high-field slope correction between 0.7 and 1 T.

Another ~100-mg portion of crushed samples was prepared for high (25°–600°C) and low (5–300 K) temperature measurements. We used a semihorizontal thermomagnetic balance to obtain thermomagnetic curves and to determine the Curie temperatures of magnetic minerals using a graphical method described by Grommé et al. (1969). Most of heating and cooling (8°C/min) runs were performed in air with a constant direct-current (DC) field of 0.75 T, but some were performed under moderate vacuum (~1 Pa) for comparison. Low-temperature magnetic properties were measured on a Quantum Design magnetic property measurement system (MPMS2). Samples were imparted at 5 K with 1-T DC field to acquire a low-temperature isothermal remanent magnetization (low-*T* IRM) and then thermally demagnetized in zero-field to room temperature.

To observe magnetic minerals and their microtextures, we used reflected-light optical polarizing microscopy and scanning electron microscopy to study polished thin sections of the cored specimens. A JEOL JSM-840A scanning electron microscope (SEM) equipped with a backscattering-electron (BSE) detector and a Link energy dispersive spectrometry (EDS) detector was used for the petrographic study and mineral identification.

## RESULTS AND DISCUSSIONS

Curie temperature data in combination with the shapes of thermomagnetic curves are characteristic of particular magnetic minerals (e.g., Dunlop and Hale, 1977; Moskowitz, 1981). Thermal demagnetization curves of low-*T* IRM can indicate the presence of minor amounts of stoichiometric magnetite (as the Verwey transition) and other magnetic phases (e.g., Özdemir et al., 1993; Moskowitz et al., 1998). Therefore, our characterization of magnetic phases in the samples is mainly based on features of thermomagnetic and low-*T* IRM demagnetization curves. The heating curves of pillow basalt samples generally show an apparent Curie temperature ranging 250°–400°C. When heated above ~300°C, the pillow basalts show one or two maxima, which probably indicate

formation of new magnetic phases and remagnetization of samples (Fig. F2A). Further heating gives leads to a Curie temperature of ~580°C. These features of thermomagnetic curves are characteristic of titanomaghemite, which becomes unstable and transforms to magnetite at elevated temperature (e.g., O'Reilly, 1984). The cooling curves are completely irreversible relative to the heating curves for the pillow basalt samples. In contrast, the massive basalt samples show almost reversible thermomagnetic curves and a Curie temperature of 170°–230°C (Fig. F2B), indicating titanomagnetite as a dominant magnetic carrier. The metadiabase sample shows approximately irreversible thermomagnetic curves with a slight maximum at 250°–300°C, which might be due to the presence of small amounts of maghemite or titanomaghemite (Fig. F2C). However, the overall heating curve gives a Curie temperature of ~580°C, indicating a predominance of magnetite in this sample.

Low-temperature magnetic properties are distinguishable among the different rock types. The pillow basalts show smooth and monotonous low-*T* IRM demagnetization curves, decreasing from 5 K to room temperature without any significant phase transition (Fig. F2A). In contrast, the massive basalts show phase transition at ~55 K (Fig. F2B). We interpret the transition at ~55 K as a possible indication of titanomagnetite (Moskowitz et al., 1998). The metadiabase sample shows phase transition at ~120 K, which is characteristic of the Verwey transition of magnetite (Fig. F2C) (Özdemir et al., 1993).

The NRM intensities of Leg 187 basalts show a wide range (0.12–16.3 A/m). The average NRM of the basalt samples for each site (or hole) ranges from 1.16 to 8.71 A/m and is equivalent to the NRM of typical ocean-ridge pillow basalts (e.g., Johnson and Hall, 1978; Beske-Diehl, 1990; Gee and Kent, 1994, 1997). This NRM range is consistent with that of oxidized pillow basalts. Although the NRM variations within one site or one hole are very large, when plotted vs. crust ages the NRM intensities show a general decreasing trend with increasing age (Fig. F3). A few sites, such as Sites 1161, 1162, and Hole 1164A have very low average NRM intensities. However, the specimens from these three sites show the highest degree of alteration among the sites (Shipboard Scientific Party, 2001) and their relatively low NRM values could be a result of pervasive alteration that has significantly modified and/or reduced concentrations of magnetic minerals. When the NRM is plotted vs. sample depth in igneous basement, it does not vary systematically with depth.

Figure F4 is a logarithmic plot of NRM vs. Curie temperature using data obtained from 43 samples. The plot shows a systematic trend of decreasing NRM with increasing Curie temperature. As Curie temperatures generally increase with increasing degrees of low-temperature oxidation (maghemitization) for oceanic basalts (e.g., O'Reilly, 1983; Zhou et al., 2001), the trend shown here implies that the degrees of maghemitization systematically increase with age in these basalts during this ~15-m.y. time span. However, a plot of Curie temperature vs. age (not shown here) does not show a clear trend of increasing Curie temperature with age. This apparent inconsistency further implies that the degree of maghemitization varies not only with age but may vary locally with the permeability of the basalts.

Table T1 contains NRM and magnetic susceptibility data for all of the analyzed specimens. Figure F5 shows two plots of NRM vs. susceptibility, with data grouped according to mantle province and tectonic zonation (Zone A or B). The plots show that both NRM and susceptibility from the different groups vary within a considerable range and neither

F2. Thermomagnetic curves and thermal demagnetization of low-*T* IRM, p. 13.

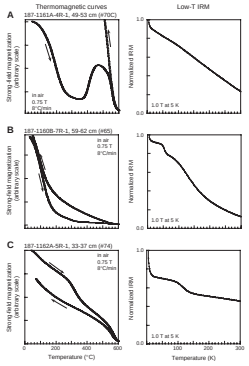


F3. NRM vs. age, p. 14.

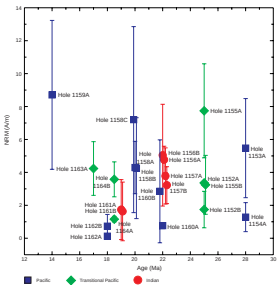


F4. NRM vs. Curie temperature, p. 15.

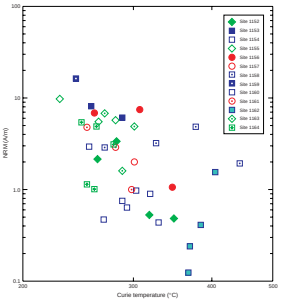


F5. NRM vs. low-field magnetic susceptibility, p. 16.

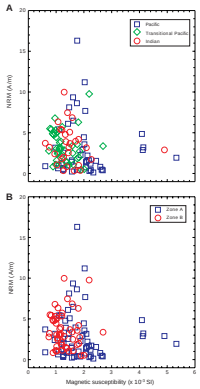

the Pacific-type samples nor the Zone A samples have, on average, higher NRM than the Indian-type or the Zone B samples. Although the amplitudes of the magnetic anomaly east of the AAD eastern boundary (Zone A) are generally much higher than those west of the AAD eastern boundary (Zone B) at the ridge area, this contrast is seen in regions only up to 46°S (e.g., Marks et al., 1990). The Leg 187 drill sites are within an area from 41° to 46°S, where the magnetic anomaly amplitudes have no significant variations between Zone A and Zone B. Our observations show no significant differences of the NRM intensities between Zone A and Zone B samples, and NRM values are consistent with the distributions of the magnetic anomaly amplitudes in this area.

Our thermal demagnetization data reveal that a stable direction persists in a majority of the pillow basalts up to ~540°C (Fig. F6A), clearly indicating that the unblocking temperatures of NRM are much higher than the Curie temperatures (250°–400°C) of titanomaghemite. We also note that a significant portion of the NRM intensity (~30%–40%) remained above the Curie temperatures. Irving (1970) suggested that this phenomenon of anomalously high unblocking temperatures relative to the Curie temperatures is caused by an artificial magnetic phase, formed as a reaction product of titanomaghemite during thermal demagnetization. However, by studying thermal demagnetization properties of very young oceanic basalts from the East Pacific Rise, Kent and Gee (1994) demonstrated that the NRM with much higher unblocking temperatures than Curie points is original and is carried by naturally occurring magnetite. Although our observations of thermal demagnetization properties for the Leg 187 pillow basalts are very similar to those of Kent and Gee (1994), our low-*T* IRM results do not support any significant Verwey transition of magnetite in the pillow basalts (Fig. F2A). Further high-resolution petrographic studies should be carried out to confirm this proposition.

During AF demagnetization, most of the pillow basalts reveal a very stable high-coercivity remanence (Fig. F6B). On the contrary, the massive basalts have a very low coercivity remanence, showing a rapid decrease in intensity and highly scattered directions at >10-mT AF demagnetization (Fig. F6C). These two types of AF demagnetization curves are typical of oceanic oxidized pillow basalts and unoxidized massive flows, respectively (Dunlop and Hale, 1976). Our results thus indicate that the majority of the Leg 187 pillow basalts are characterized by a single stable component of remanence, whereas the coarse-grained massive basalts readily acquire components of viscous remanence, consistent with the results of previous rock magnetic studies on oceanic basalts (e.g., Dunlop and Hale, 1976; Johnson and Hall, 1978). The AF demagnetization results also suggest that the grain sizes of magnetic carriers in the pillow basalts should be much smaller than those in the massive basalts (see below).

The granulometry of magnetic minerals can generally be inferred from the hysteresis loops and Day plot ($M_{rs}/M_s$ vs. $B_{cr}/B_c$; Day et al., 1977). The hysteresis loops obtained from the specimens of three major rock types are shown in Figure F7. Hysteresis parameters of all specimens are listed in Table T1, and their Day plots are shown in Figure F8. The hysteresis loops of the pillow basalt samples generally show wasp-waisted or constricted shape (Fig. F7A), suggesting that the magnetic mineral is possibly composed of a mixture of superparamagnetic (SP) and stable single-domain (SSD) grains (Dunlop and Özdemir, 1997; Gee and Kent, 1999). Most of the Leg 187 specimens have $M_{rs}/M_s$ = 0.40–

F6. Demagnetization diagrams, p. 17.

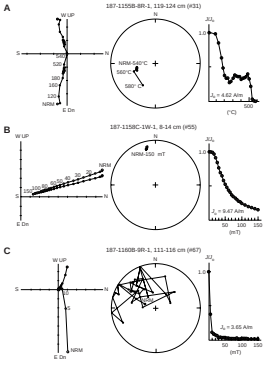

F7. Hysteresis loops for basalts, p. 18.

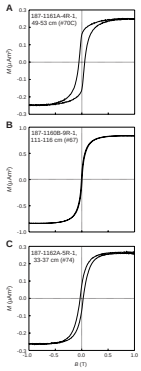

F8. Day plots for basalts of the three mantle types, p. 19.

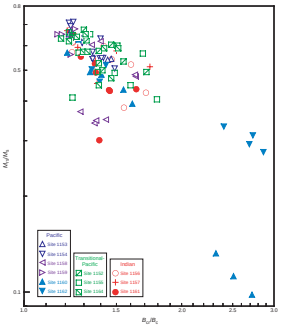

0.70 and $B_{cr}/B_c$ = 1.2–2.0. It should be noted that more than one-half of the $M_{rs}/M_s$ ratios plot above 0.5, which is a theoretical limit for uniaxial anisotropy (Dunlop and Özdemir, 1997). Our data indicate that the magnetic minerals in the Leg 187 basalts are predominantly of cubic anisotropy, which is the same as that demonstrated for a broad collection of oceanic basalts by Gee and Kent (1999). On the basis of the Day plot and hysteresis loops, the titanomaghemite contained in the dominant pillow basalt samples ranges from SSD to pseudosingle-domain (PSD) grains (Figs. **F7, F8**). Magnetic grains are larger in the massive basalts from Hole 1160B than those in the pillow basalts because their data points on the Day plot are closer to the multidomain category (larger PSD). The massive basalt samples have low coercivity ($B_c$) but relatively high susceptibility and saturation magnetization ($M_s$) (Table **T1**). The metadiabase sample from Hole 1162A also plots in the larger PSD category (Fig. **F8**).

The petrographic observations of polished thin sections under SEM are consistent with the results inferred from magnetic properties. Most pillow basalt samples contain very fine grained skeletal or subhedral titanomagnetite (a few micrometers in diameter to ~10 µm in long dimension), which occurs as an interstitial phase between plagioclase and clinopyroxene grains (Fig. **F9A**). The massive basalt samples from Hole 1160B contain subhedral to euhedral titanomagnetite up to tens of micrometers in size (Fig. **F9B**). These titanomagnetite grains do not show any distinguishable internal textural features that might be caused by alteration or oxidation. Therefore, the dominant magnetic carrier in the massive basalts is primary titanomagnetite with relatively larger grain sizes, consistent with their magnetic properties, such as low coercivity and low Curie temperature. The metadiabase sample from Hole 1162A contains subhedral titanomagnetite pseudomorphs (up to a few hundred micrometers across) with well-oriented ilmenite lamellae (Fig. **F9C**). This lamellar texture is characteristic of "oxidation-exsolution" or high-temperature oxidation, to which the titanomagnetite was subjected and which, together with pervasive hydrothermal alteration, gave rise to end-member magnetite as the magnetic carrier in this rock type (e.g., Shau et al., 1993, 2000). The effective grain size of the magnetite is significantly reduced due to the crosscutting of primary titanomagnetite by ilmenite lamellae.

The titanomagnetite grains in the pillow basalt samples are indeed pseudomorphs, which have presumably been subjected to different degrees of low-temperature oxidation and changed into titanomaghemite. That the titanomagnetite underwent low-temperature oxidation is not indicated only by the relatively high Curie temperatures and irreversible thermomagnetic curves for these pillow basalt samples, but also by the shrinkage curvature cracks that are commonly seen in titanomagnetite pseudomorphs from the oldest samples from Leg 187 (e.g., samples from Sites 1154 and 1152) (Fig. **F10A**). The curvature cracks are a diagnostic feature for the presence of titanomaghemite, which formed after titanomagnetite via maghemitization and with a volume change (e.g., Johnson and Hall, 1978). The formation of shrinkage cracks might divide the titanomagnetite grains into submicroscopic grains. The shrinkage cracks are most abundant in titanomagnetite pseudomorphs from the oldest samples of Leg 187 but are not clearly visible in those of the younger samples. This observation is consistent with the above argument that the degree of maghemitization systematically increases with age. However, the younger basalt samples still contain titanomaghemite, as shown by their Curie temperatures and irreversible

**F9.** Petrographic features of different rock types, p. 20.

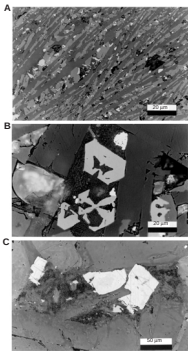

**F10.** Features of opaque minerals, p. 21.

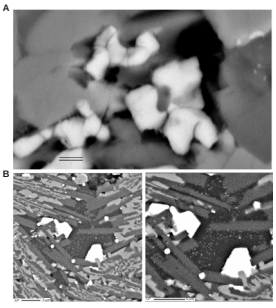

thermomagnetic curves. Under higher magnification, we found that many submicroscopic Fe-Ti oxide mineral grains are present within the interstitial glass of many pillow basalts (Fig. F10B). The sizes of these submicroscopic magnetic mineral grains are much smaller than 0.5 µm and are consistent with the relatively large $M_{rs}/M_s$ ratios and SSD grains inferred from the Day plot.

Table T2 summarizes the Leg 187 core samples with respect to rock types, magnetic minerals, magnetic properties, and alteration features. Most core samples are pillow basalts that contain titanomaghemite as the main magnetic carrier and are characterized by a single stable component of remanence. Three massive basalt samples contain nearly unoxidized titanomagnetite, and a metadiabase sample contains secondary magnetite as its dominant magnetic carrier.

T2. Magnetic properties of the three rock types, p. 25.

The NRM intensities of MORB may vary in relation to several factors such as geomagnetic field intensity (e.g., Ravilly et al., 2001), concentration of magnetic minerals (mainly titanomagnetite), which is in turn related to rock chemistry (e.g., Marshall and Cox, 1972; Gee and Kent, 1997), and grain size of magnetic minerals (e.g., Marshall and Cox, 1971; Ryall and Ade-Hall, 1975; Gee and Kent, 1997). Significant variations of NRM vs. distance from pillow margins have been demonstrated in relatively young and zero-age MORB (e.g., Marshall and Cox, 1971; Ryall and Ade-Hall, 1975; Gee and Kent, 1997). Ryall and Ade-Hall (1975) showed significant radial variations of NRM intensity in 0- to 286-ka pillows and very uniform NRM intensities vs. distance from margin of a 740-ka pillow basalt except in the first few millimeters of the pillow rinds. As the MORB drilled during Leg 187 is 14–28 Ma, we expect that the radial variations of NRM intensities will be much less significant. However, in order to decrease the possible radial variations and compare the NRM intensities among samples from different sites and holes from Leg 187, we collected samples for our magnetic measurements in a similar depth range at ~0.5 cm from pillow margins for the rim samples and ~1–3 cm from pillow margins for the core samples.

The Leg 187 basalt samples show a general decreasing trend of NRM with increasing crust ages from 14 to 28 Ma. This trend might indicate an increasing degree of low-temperature oxidation (e.g., Johnson and Pariso, 1993; Zhou et al., 2001) or reflect decreasing concentration of magnetic minerals due to increasing degree of alteration (e.g., Xu et al., 1997). Our data show that NRM intensities correlate reciprocally with the Curie temperatures (Fig. F4). In addition, when considering a larger time span, the Curie temperatures (250°–400°C) of the Leg 187 pillow basalts are significantly higher than those from the very young MORB. For example, Gee and Kent (1997) showed Curie temperatures ranging 100°–240°C for most of the zero-age basalts collected from the southern East Pacific Rise. This contrast in the Curie temperatures indicates that the older Leg 187 basalts were subjected to much higher degrees of low-temperature oxidation. We therefore infer that the general trend of decreasing NRM intensities with age in the Leg 187 basalts reflects an increasing degree of low-temperature oxidation. However, as mentioned previously, a plot of Curie temperature vs. sample age does not unambiguously show a positive relationship between the degree of low-temperature oxidation and crust ages. This led us to believe that, in addition to the factor of timing (crust ages), the large variations of NRM are mainly controlled by local variations of the extent of low-temperature oxidation, which is closely dependent on the permeability of the basalts. The presence of nearly unoxidized titanomagnetite in the massive basalts also indicates that the permeability of rocks is a main con-

trolling factor to maghemitization. This is consistent with the observations by Johnson and Hall (1978), in which they showed that the impermeable massive flows from the Nazca plate can remain unoxidized for as long as 40 m.y.

The NRM of the dominant pillow basalt samples from Leg 187 probably originated from a primary TRM acquired during basaltic subsolidus cooling and from a CRM that modified the TRM during low-temperature oxidation and alteration. Recent studies have shown that the NRM of MORB can be partially contributed from unoxidized, very fine grained titanomagnetite in the interstitial glass (Zhou et al., 1997, 1999, 2000, 2001). Although we have also observed very fine grained Fe-Ti oxide minerals in the interstitial glass of the Leg 187 pillow basalt samples (Fig. **F10B**), the resolution of the SEM is not high enough to characterize their composition and texture. Further study on the magnetic minerals in these basalt samples will be carried out using a high-resolution transmission electron microscopy (TEM).

## SUMMARY

The dominant magnetic carrier in the SEIR pillow basalts recovered during Leg 187 is titanomaghemite, which presumably formed via low-temperature oxidation (maghemitization) of primary titanomagnetite. Few massive basalt samples contain nearly unoxidized titanomagnetite, indicating that permeability of rocks is a primary controlling factor of maghemitization. The pillow basalts contain titanomaghemite ranging from SSD to PSD grains and are characterized by a single stable component of remanence. The massive basalts contain titanomagnetite that is larger PSD grains.

The NRM values for the SEIR basalts are on the same order as those for other oceanic basalts. They show a general decreasing trend of NRM with crust age from ~14 to ~28 Ma, which reflects an increasing degree of low-temperature oxidation. The magnetic properties, including NRM, of the cored samples recovered from very shallow levels of the pillow layers do not correlate either with tectonic zonations or with mantle provinces of the samples.

## ACKNOWLEDGMENTS

This research used samples provided by the Ocean Drilling Program (ODP). The ODP is sponsored by the U.S. National Science Foundation (NSF) and participating countries under management of Joint Oceanographic Institutions (JOI), Inc. The authors are grateful to the Leg 187 Shipboard Scientific Party and shipboard specialists for their help. We are grateful to Miguel Garcés, Jeff Gee, and Jay Miller for their constructive reviews and helpful comments that greatly improved the manuscript. We thank N. Ishikawa of Kyoto University for the use of the MicroMag and thermomagnetic balance, M. Fukuhara of Okayama University of Science for the use of the MPMS, and H.-Y. Yang of National Cheng Kung University for the use of the JEOL JSM-840A SEM. We also thank S.-F. Ou for helping measure rock magnetic properties and H.-D. Jiang for his technical assistance with BSE imaging. This study was supported by NSC grants NSC89-2611-M-110-028-ODP and NSC90-2611-M-110-006-ODP to Y.-H.S.

## REFERENCES

Anderson, R.N., Spariosu, D.J., Weissel, J.K., and Hayes, D.E., 1980. The interpretation between variations in magnetic anomaly amplitudes and basalt magnetization and chemistry along the Southeast Indian Ridge. *J. Geophys. Res.,* 85:3883–3898.

Beske-Diehl, S.J., 1990. Magnetization during low-temperature oxidation of seafloor basalts: no large scale chemical remagnetization. *J. Geophys. Res.,* 95:21413–21432.

Christie, D.M., Pedersen, R.B., Miller, D.J., et al., 2001. *Proc. ODP, Init. Repts.,* 187 [CD-ROM]. Available from: Ocean Drilling Program, Texas A&M University, College Station TX 77845-9547, USA.

Christie, D.M., West, B.P., Pyle, D.G., and Hanan, B.B., 1998. Chaotic topography, mantle flow and mantle migration in the Australian-Antarctic Discordance. *Nature,* 394:637–644.

Day, R., Fuller, M., and Schmidt, V.A., 1977. Hysteresis properties of titanomagnetites: grain-size and compositional dependence. *Phys. Earth Planet. Inter.,* 13:260–267.

Dunlop, D.J., and Hale, C.J., 1976. A determination of paleomagnetic field intensity using submarine basalts drilled near the Mid-Atlantic Ridge. *J. Geophys. Res.,* 81:4166–4172.

————, 1977. Simulation of long-term changes in the magnetic signal of the oceanic crust. *Can. J. Earth Sci.,* 14:716–744.

Dunlop, D.J., and Özdemir, Ö., 1997. *Rock Magnetism: Fundamentals and Frontiers:* Cambridge (Cambridge Univ. Press).

Gee, J., and Kent, D.V., 1994. Variations in Layer 2A thickness and the origin of the central anomaly magnetic high. *Geophys. Res. Lett.,* 21:297–300.

————, 1997. Magnetization of axial lavas from the southern East Pacific Rise (14°–23°S): geochemical controls on magnetic properties. *J. Geophys. Res.,* 102:24873–24886.

————, 1999. Calibration of magnetic granulometry trends in oceanic basalts. *Earth Planet. Sci. Lett.,* 170:377–390.

Grommé, C.S., Wright, T.L., and Peck, D.L., 1969. Magnetic properties and oxidation of iron-titanium oxide minerals in Alae and Makaopuhi lava lakes, Hawaii. *J. Geophys. Res.,* 74:5277–5293.

Hall, J.M., and Muzzatti, A., 1999. Delayed magnetization of the deeper kilometer of oceanic crust at Ocean Drilling Project Site 504. *J. Geophys. Res.,* 104:12843–12851.

Hayes, D.E., and Conolly, J.R., 1972. Morphology of the Southeast Indian Ocean. *In* Hayes, D.E. (Ed.), *Antarctic Oceanology* (Vol. 2). Antarct. Res. Ser., 19:125–145.

Irving, E., 1970. The Mid-Atlantic Ridge at 45°N. XIV. Oxidation and magnetic properties of basalt; review and discussion. *Can. J. Earth Sci.,* 7:1528–1538.

Johnson, H.P., and Hall, J.M., 1978. A detailed rock magnetic and opaque mineralogy study of the basalts from the Nazca plate. *Geophys. J. R. Astron. Soc.,* 52:45–64.

Johnson, H.P., and Pariso, J.E., 1993. Variations in oceanic crustal magnetization: systematic changes in the last 160 million years. *J. Geophys. Res.,* 98:435–445.

Johnson, H.P., and Tivey, M.A., 1998. A re-evaluation of a contribution to marine magnetic anomalies from lower crustal rocks. *Eos, Trans. Am. Geophys. Union,* 79:F230.

Kent, D.V., and Gee, J., 1994. Grain size-dependent alteration and the magnetization of oceanic basalts. *Science,* 265:1561–1563.

Klein, E.M., Langmuir, C.H., Zindler, A., Staudigel, H., and Hamelin, B., 1988. Isotope evidence of a mantle convection boundary at the Australian-Antarctic Discordance. *Nature,* 333:623–629.

Marks, K.M., Vogt, P.R., and Hall, S.A., 1990. Residual depth anomalies and the origin of the Australian-Antarctic Discordance Zone. *J. Geophys. Res.,* 95:17325–17337.

Marshall, M., and Cox, A., 1971. Magnetism of pillow basalts and their petrology. *Geol. Soc. Am. Bull.,* 82:537–552.

————, 1972. Magnetic changes in pillow basalts due to seafloor weathering. *J. Geophys. Res.,* 77:6459–6469.

Moskowitz, B.M., 1981. Methods for estimating Curie temperatures of titanomaghemites from experimental $J_s$-T data. *Earth Planet. Sci. Lett.,* 53:84–88.

Moskowitz, B.M., Jackons, M., and Kissel, C., 1998. Low-temperature magnetic behavior of titanomagnetites. *Earth Planet. Sci. Lett.,* 157:141–149.

O'Reilly, W., 1983. The identification of titanomagnetites: model mechanisms for the maghemitzation and inversion process and their magnetic consequences. *Phys. Earth Planet. Inter.,* 31:65–76.

————, 1984. *Rock and Mineral Magnetism:* New York (Chapman and Hall).

Özdemir, Ö., Dunlop, D.J., and Moskowitz, B.M., 1993. The effect of oxidation on the Verwey transition in magnetite. *Geophys. Res. Lett.,* 20:1671–1674.

Pyle, D.G., Christie, D.M., and Mahoney, J.J., 1992. Resolving an isotopic boundary within the Australian-Antarctic Discordance. *Earth Planet. Sci. Lett.,* 112:161–178.

Ravilly, M., Horen, H., Perrin, M., Dyment, J., Gente, P., and Guillou, H., 2001. NRM intensity of altered oceanic basalts across the MAR (21°N, 0–1.5 Ma): a record of geomagnetic paleointensity variations? *Geophys. J. Int.,* 145:401–422.

Ryall, P.J.C., and Ade-Hall, J.M., 1975. Radial variation of magnetic properties in submarine pillow basalts. *Can. J. Earth Sci.,* 12:1959–1969.

Shau, Y.-H., Peacor, D.R., and Essene, E.J., 1993. Formation of magnetic single-domain magnetite in ocean ridge basalts with implications for seafloor magnetism. *Science,* 261:343–345.

Shau, Y.-H., Torii, M., Horng, C.-S., and Peacor, D.R., 2000. Subsolidus evolution and alteration of titanomagnetite in ocean ridge basalts from Deep Sea Drilling Project/Ocean Drilling Program Hole 504B, Leg 83: implications for the timing of magnetization. *J. Geophys. Res.,* 105:23635–23649.

Shipboard Scientific Party, 2001. Leg 187 summary. *In* Christie, D.M., Pedersen, R.B., Miller, D.J., et al., *Proc. ODP, Init. Repts.,* 187: College Station TX (Ocean Drilling Program), 1–49.

Vine, F.J., and Matthews, D.H., 1963. Magnetic anomalies over oceanic ridges. *Nature,* 199:947–949.

Vogt, P.R., Cherkis, N.Z., and Morgan, G.A., 1983. Project investigator—1. Evolution of the Australian-Antarctic discordance deduced from a detailed aeromagnetic study. *In* Oliver, R.L., James, P.R., and Jago, J.B. (Eds.), *Antarctic Earth Science.* Proc. 4th Internat. Symp. Antarctic Earth Sci., 608–613.

Weissel, J.K., and Hayes, D.E., 1971. Asymmetric seafloor spreading south of Australia. *Nature,* 231:518–522.

Xu, W., Van der Voo, R., Peacor, D.R., and Beaubouef, R., 1997. Alteration and dissolution of fine-grained magnetite and its effects on magnetization of the ocean floor. *Earth Planet. Sci. Lett.,* 151:279–288.

Zhou, W., Van der Voo, R., and Peacor, D.R., 1997. Single-domain and superparamagnetic titanomagnetite with variable Ti content in young ocean-floor basalts: no evidence for rapid alteration. *Earth Planet. Sci. Lett.,* 150:353–361.

————, 1999. Preservation of pristine titanomagnetite in older ocean-floor basalts and its significance for paleointensity studies. *Geology,* 27:1043–1046.

Zhou, W., Van der Voo, R., Peacor, D.R., Wang, D., and Zhang, Y., 2001. Low-temperature oxidation of titanomagnetite to titanomaghemite in MORB: a gradual process with implications for marine magnetic anomaly amplitudes. *J. Geophys. Res.,* 106:6409–6421.

Zhou, W., Van der Voo, R., Peacor, D.R., and Zhang, Y., 2000. Variable Ti-content and grain size of titanomagnetite as a function of cooling rate in very young MORB. *Earth Planet. Sci. Lett.,* 179:9–20.

**Figure F1.** Locations of Leg 187 drill sites. Mantle provinces for each site are indicated. The Southeast Indian Ridge is shown as double heavy black lines, major fracture zones as brown dashed lines, and seafloor isochrons (Vogt et al., 1984) as thin gray lines. The Zone A and Zone B (the Australian Antarctic Discordance; AAD) tectonic segments extend to 140° and 120°E, respectively. The core samples were recovered from 23 holes at the 13 drill sites (Sites 1152–1164) with an average water depth of ~5000 m. The coring depth ranges from 20–60 m into the igneous basement (after figure F27, Shipboard Scientific Party, 2001).

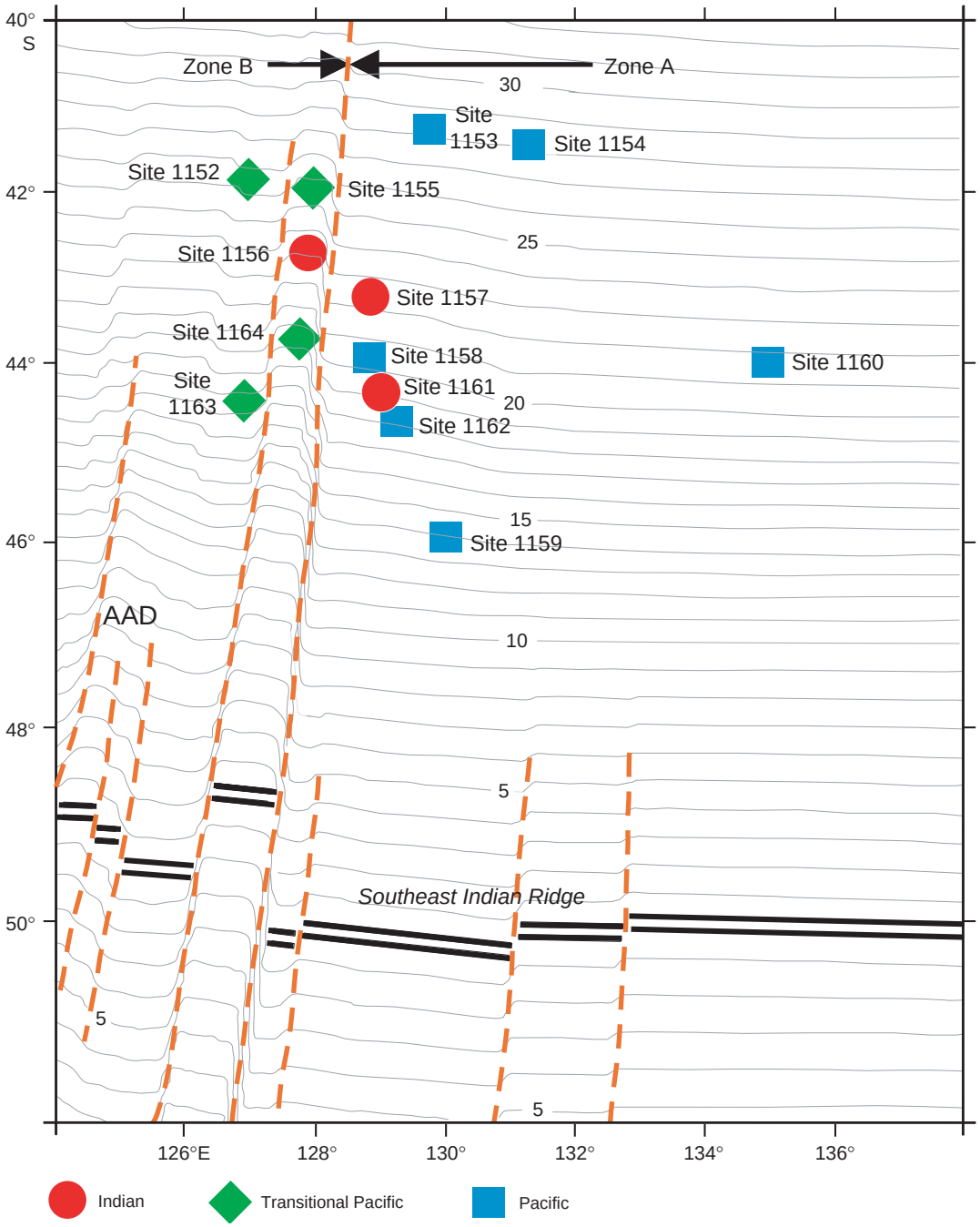

**Figure F2.** Representative thermomagnetic curves (left column) and thermal demagnetization of low-*T* isothermal remanent magnetization (IRM) (right column) for three types of Leg 187 samples. **A.** Pillow basalt: thermomagnetic curve on heating shows Curie temperature at ~250°C and a reaction maximum at elevated temperature; cooling curve is irreversible; low-*T* IRM curve is monotonous. **B.** Massive flow: almost reversible thermomagnetic curves showing ~170°C Curie temperature; low-*T* IRM curve showing stepping down at ~55 K. **C.** Metadiabase: thermomagnetic curves showing two Curie points at ~370° and ~580°C; low-*T* IRM curve showing phase transition at ~120 K. Vertical axis for the strong-field magnetization is arbitrary and that for low-*T* IRM is normalized for the value at 5 K.

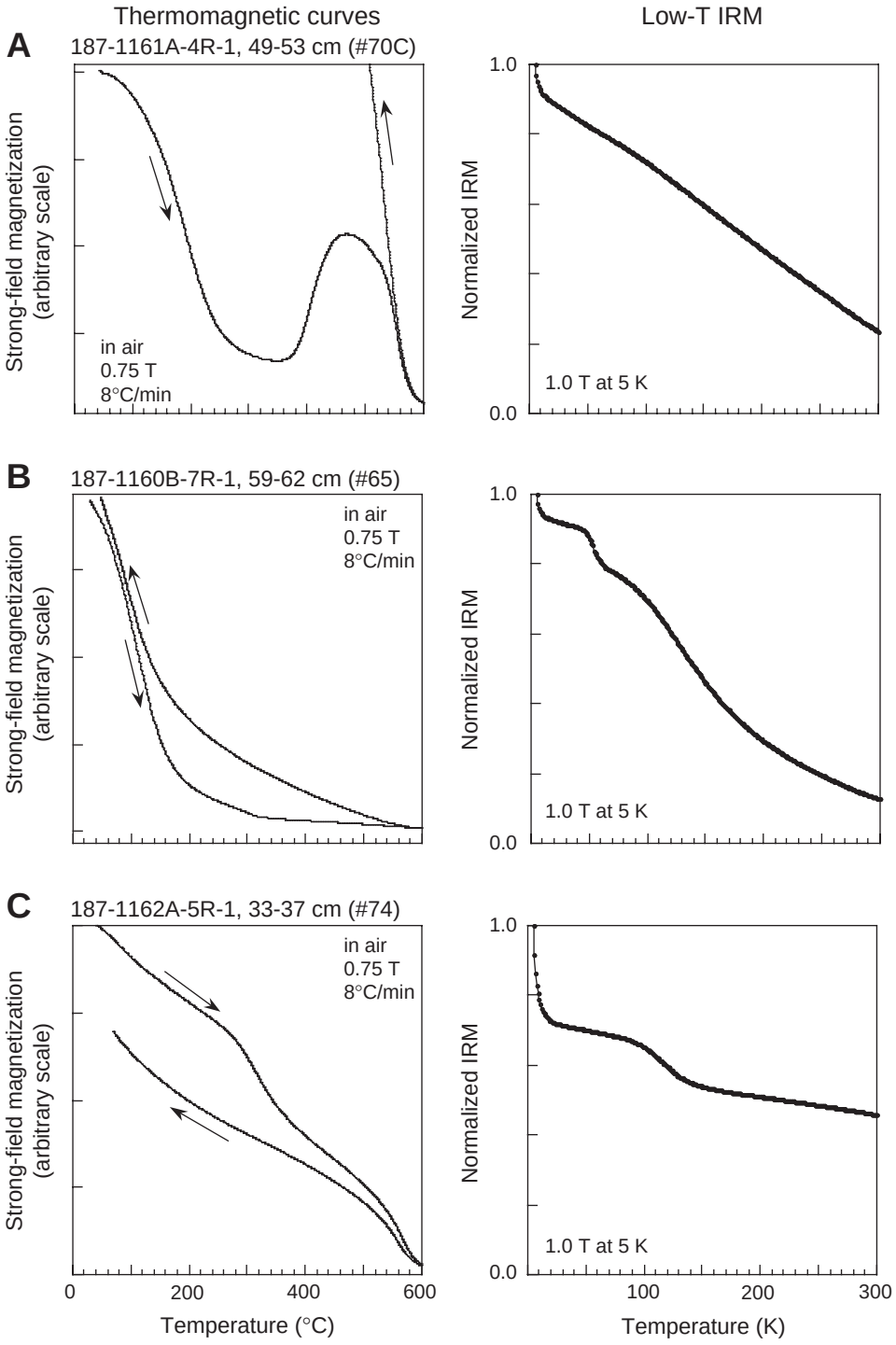

**Figure F3.** Natural remanent magnetization (NRM) vs. age for Leg 187 basalt samples. Plots and conjugated error bars indicate average NRM and one standard deviation, respectively. Plots for the holes of the same ages are slightly deviated horizontally for clarity.

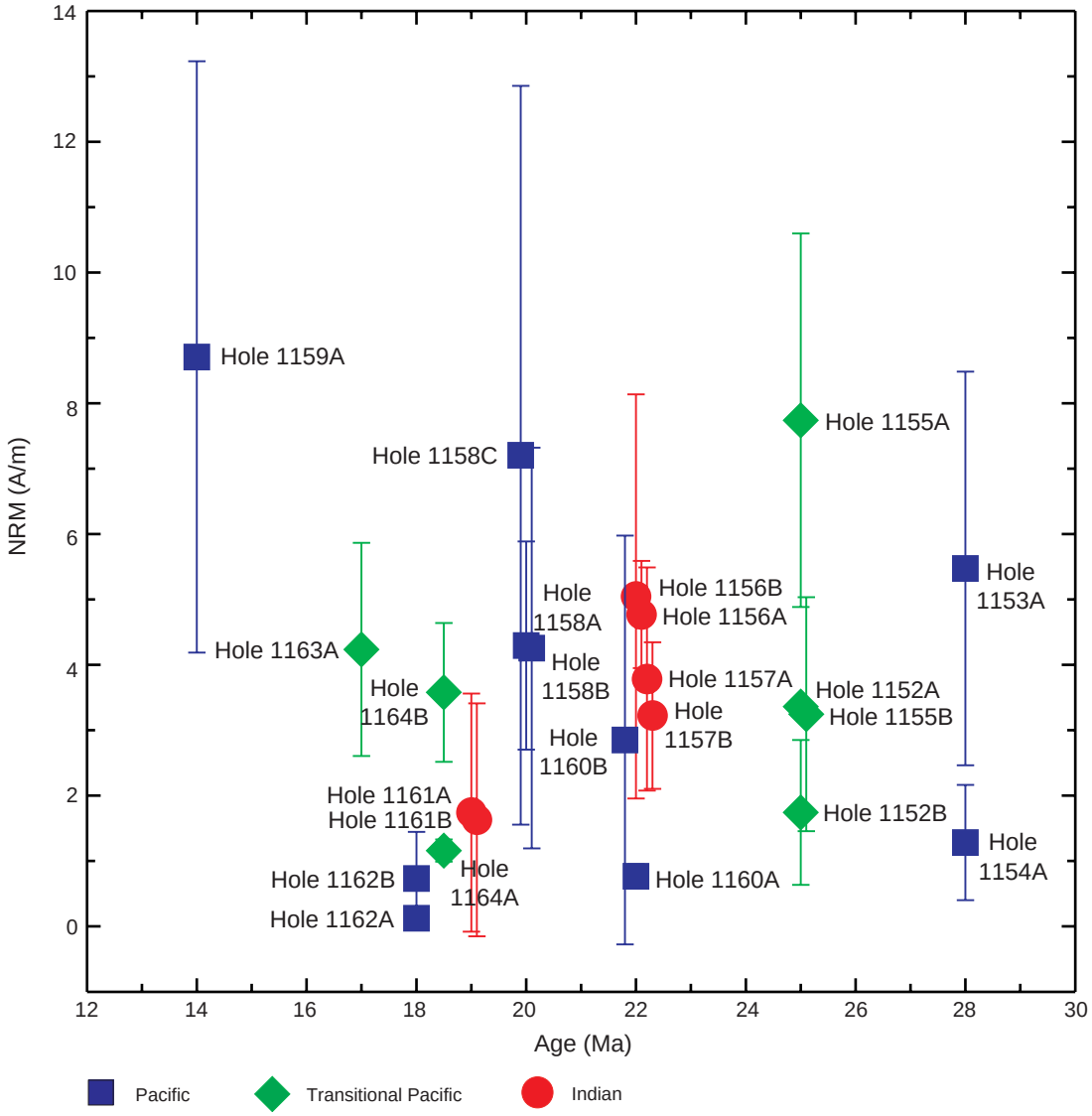

**Figure F4.** Logarithmic plot of natural remanent magnetization (NRM) vs. Curie temperature of the Leg 187 basalt samples.

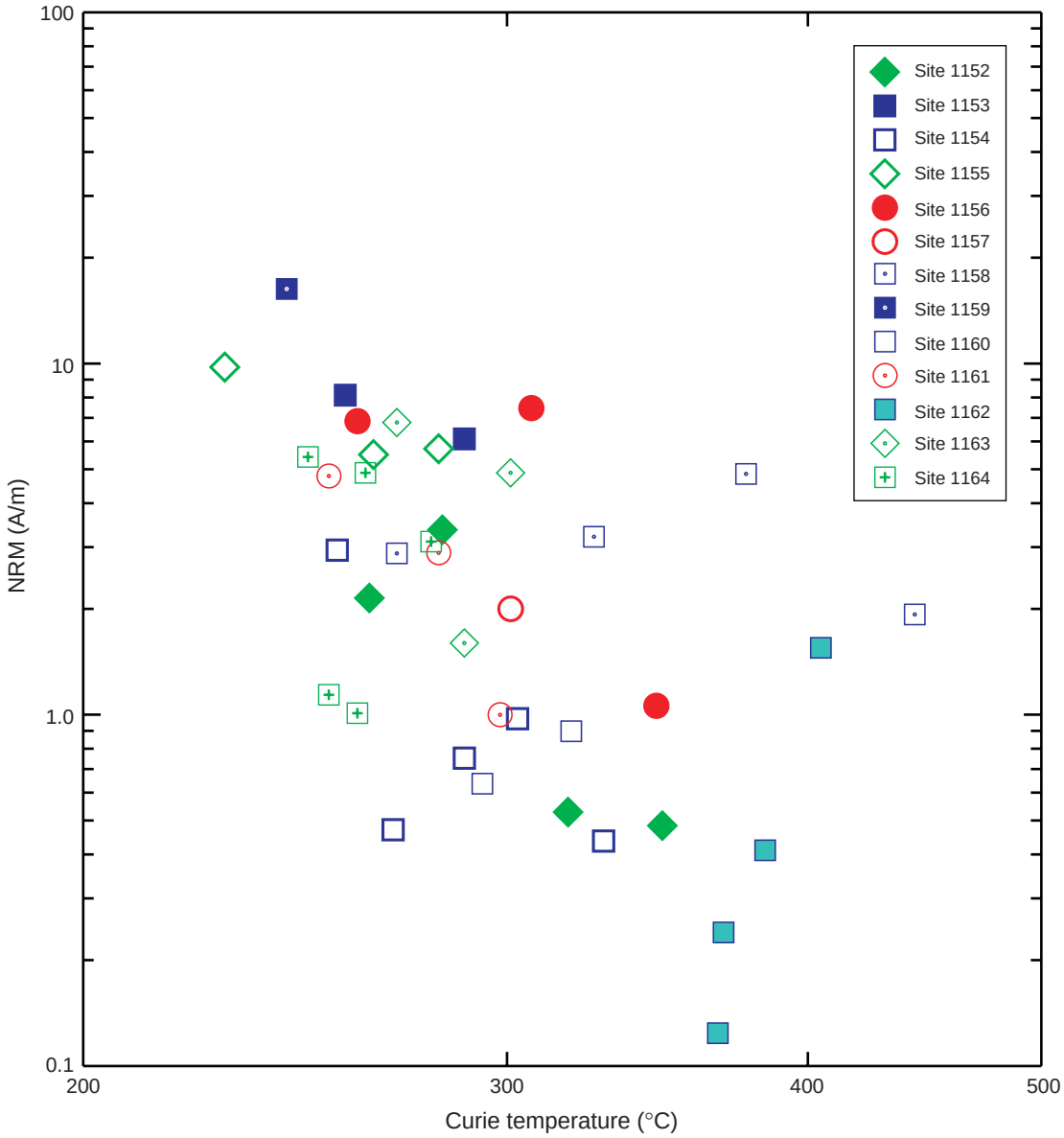

**Figure F5.** Natural remanent magnetization (NRM) vs. low-field magnetic susceptibility (volume specific) of the Leg 187 basalt samples, which are grouped according to (**A**) mantle provinces and (**B**) tectonic zonations. Three data points from the massive basalt samples with susceptibility values ranging from $15 \times 10^{-3}$ to $25 \times 10^{-3}$ SI are outside the plot area.

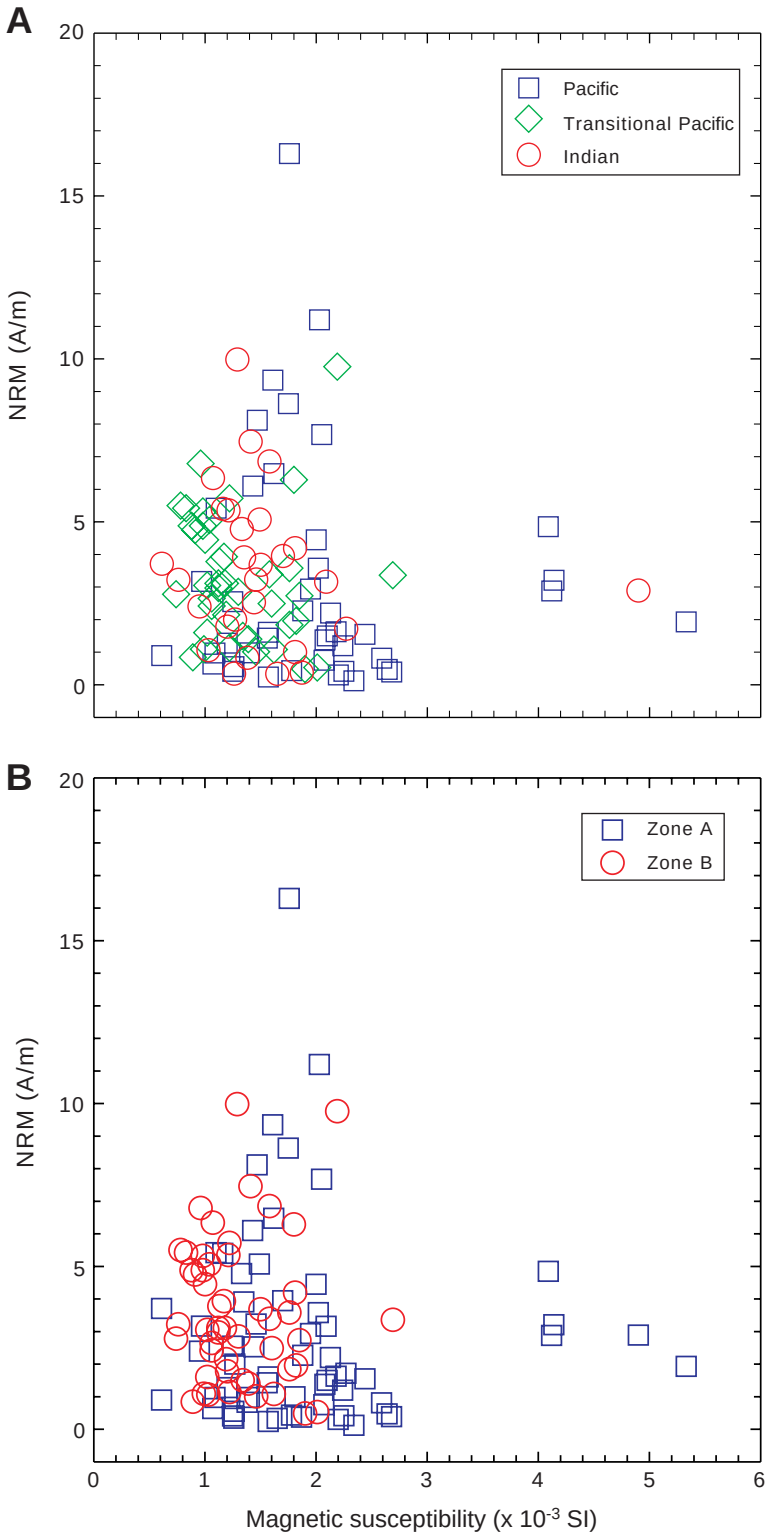

**Figure F6.** Representative demagnetization diagrams of Leg 187 samples. The samples were not oriented. **A.** Thermal demagnetization of pillow basalts, showing a stable direction of natural remanent magnetization (NRM) and high unblocking temperatures up to ~540°C. **B.** AF demagnetization of pillow basalts, revealing a very stable high-coercivity remanence up to 150 mT. **C.** AF demagnetization of massive basalts, showing a rapid decreasing in intensity and highly scattered directions when AF demagnetization is >10 mT.

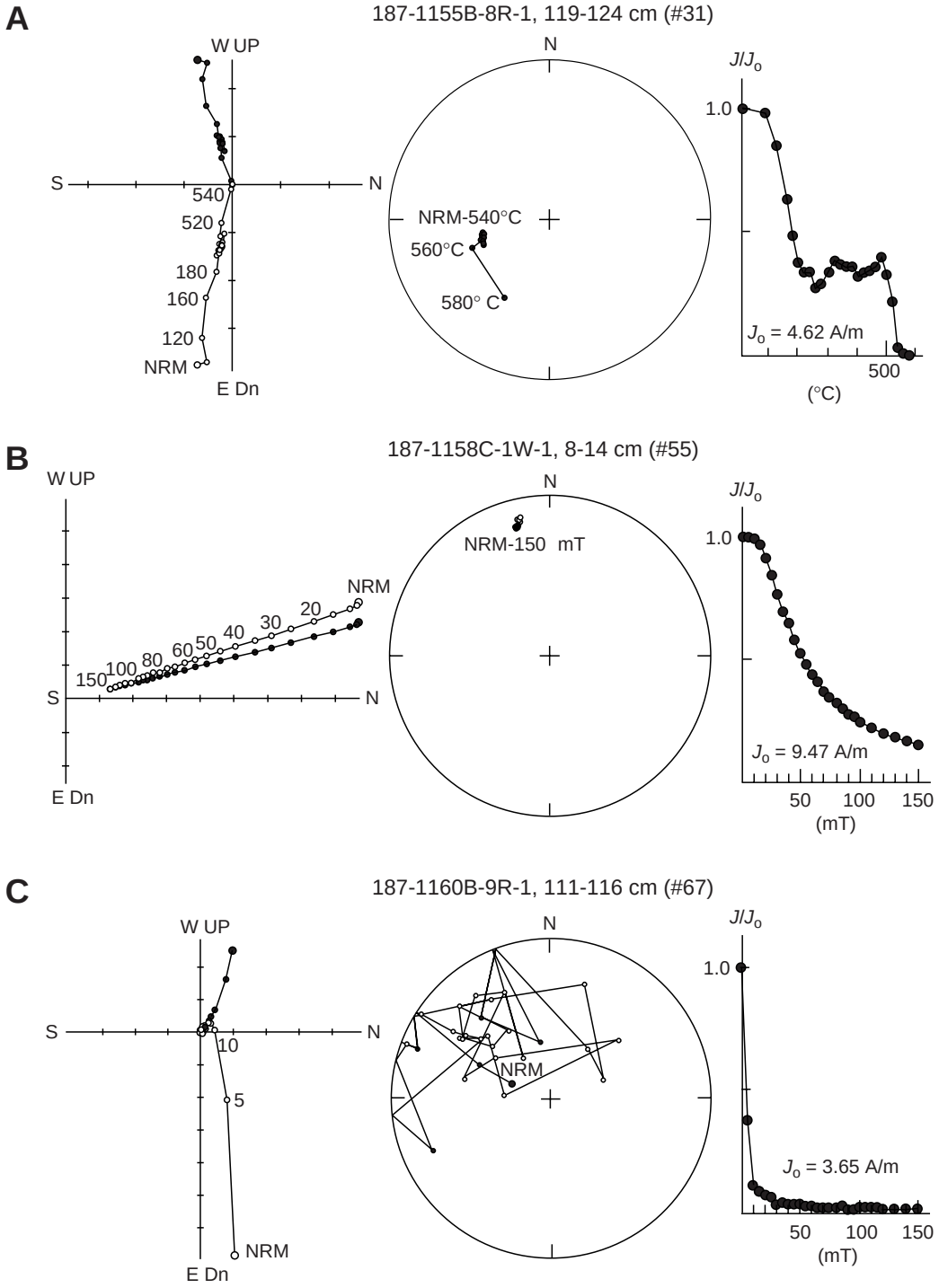

**Figure F7.** Hysteresis loops of (**A**) a pillow basalt, (**B**) a massive basalt, and (**C**) a metadiabase from ODP Leg 187. *M* = magnetization, *B* = applied magnetic field.

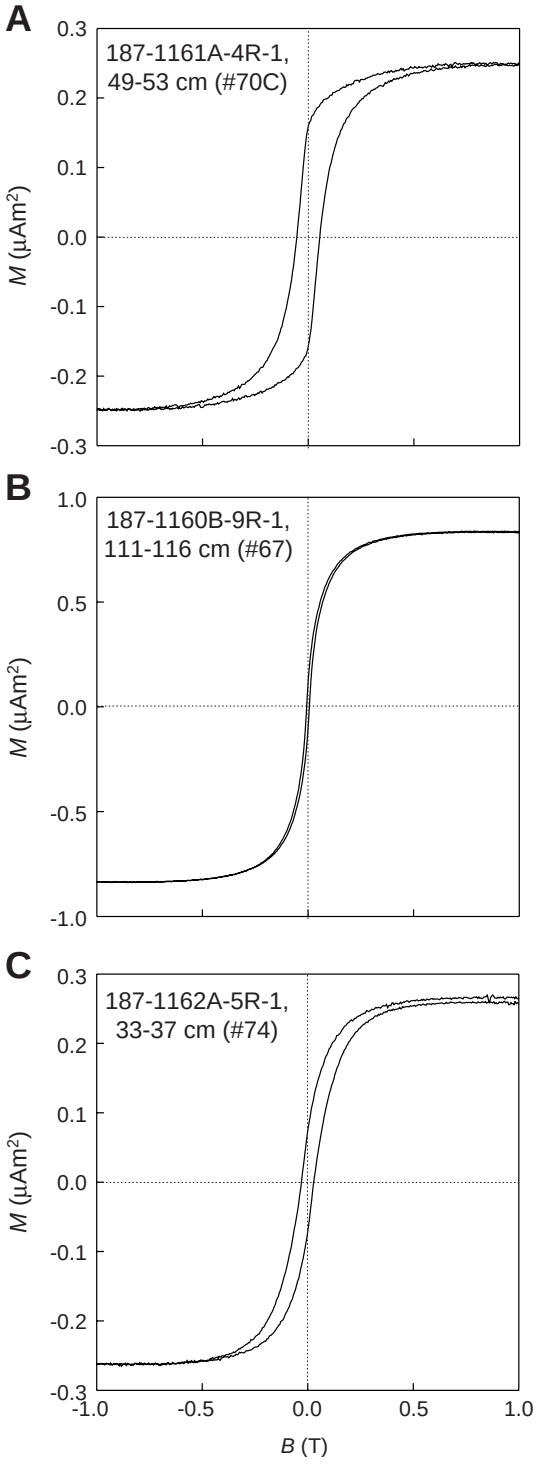

**Figure F8.** Hysteresis ratios $M_{rs}/M_s$ vs. $B_{cr}/B_c$ plots (Day plots) for the Pacific-type, Transitional-Pacific-type, and Indian-type basalts from Leg 187, showing that most of the samples contain magnetic minerals ranging from SSD to PSD sizes. Plots of data for Site 1163 are incorporated with Site 1164. Three solid triangles plotted at the lowest right corner are the three massive basalt samples (#63, #65, and #67) from Hole 1160B. Four upside-down solid triangles plotted at the middle right side are four data points from the metadiabase sample (#74) from Hole 1162A. $M_s$ = saturation magnetization, $M_{rs}$ = saturation remanent magnetization, $B_c$ = coercivity, $B_{cr}$ = remanent coercivity.

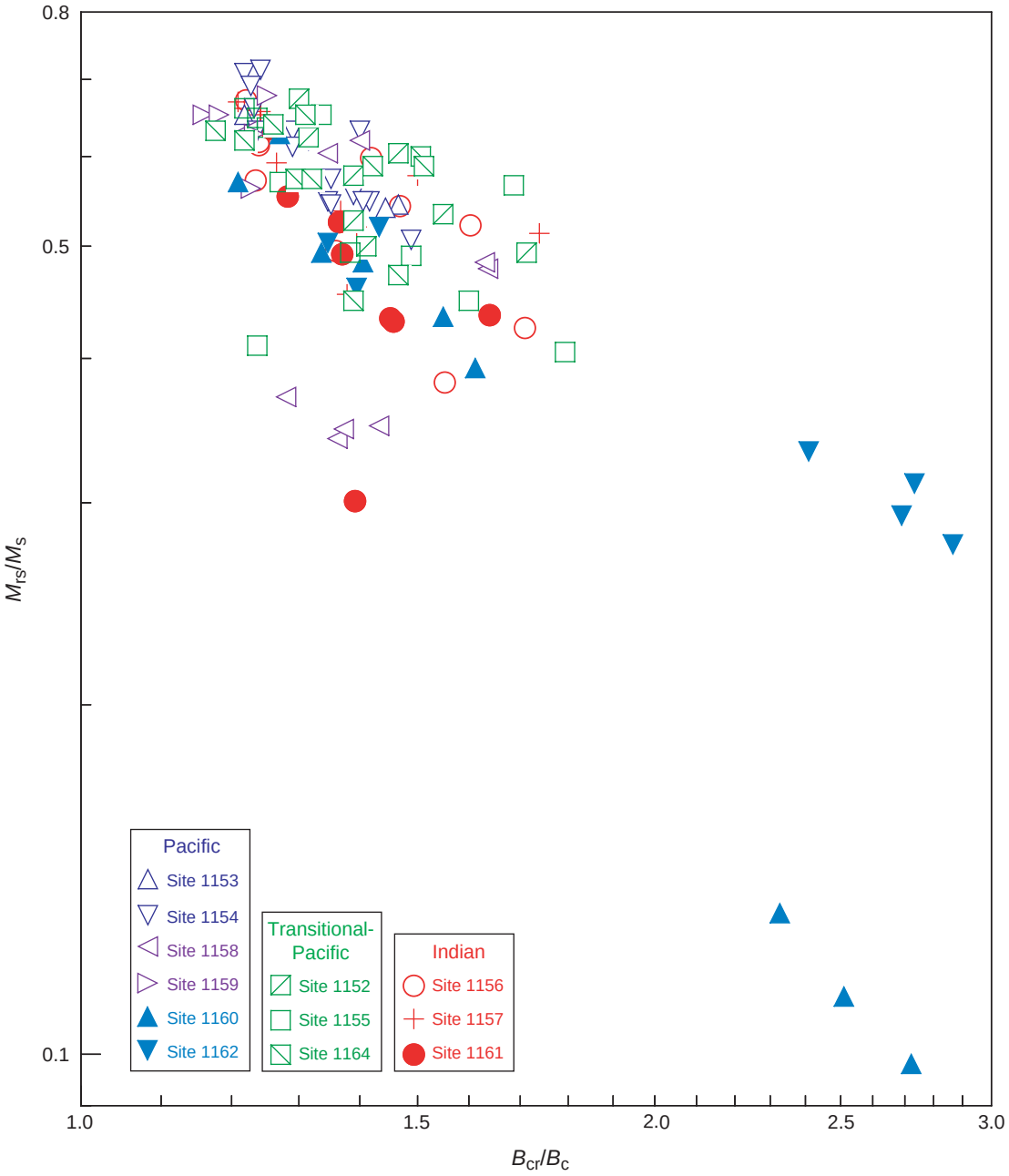

**Figure F9.** Scanning electron microscopic backscattered electron images showing petrographic features of different rock types from Leg 187 samples. **A.** Fe-Ti oxide minerals (white contrast), clinopyroxene (light gray), and plagioclase (dark gray) in pillow basalt (Sample 187-1159A-2R-1, 26–30 cm [#57]). **B.** Titanomagnetite (tan contrast) and iron sulfides (extra bright) occur between thick plagioclase laths in massive basalt (Sample 187-1160B-9R-1, 111–116 cm [#67]). **C.** Titanomagnetite pseudomorphs showing well-oriented lamellae in metadiabase (Sample 187-1162A-5R-1, 33–37 cm [#74]). The areas surrounding the titanomagnetite pseudomorphs contain abundant secondary actinolite.

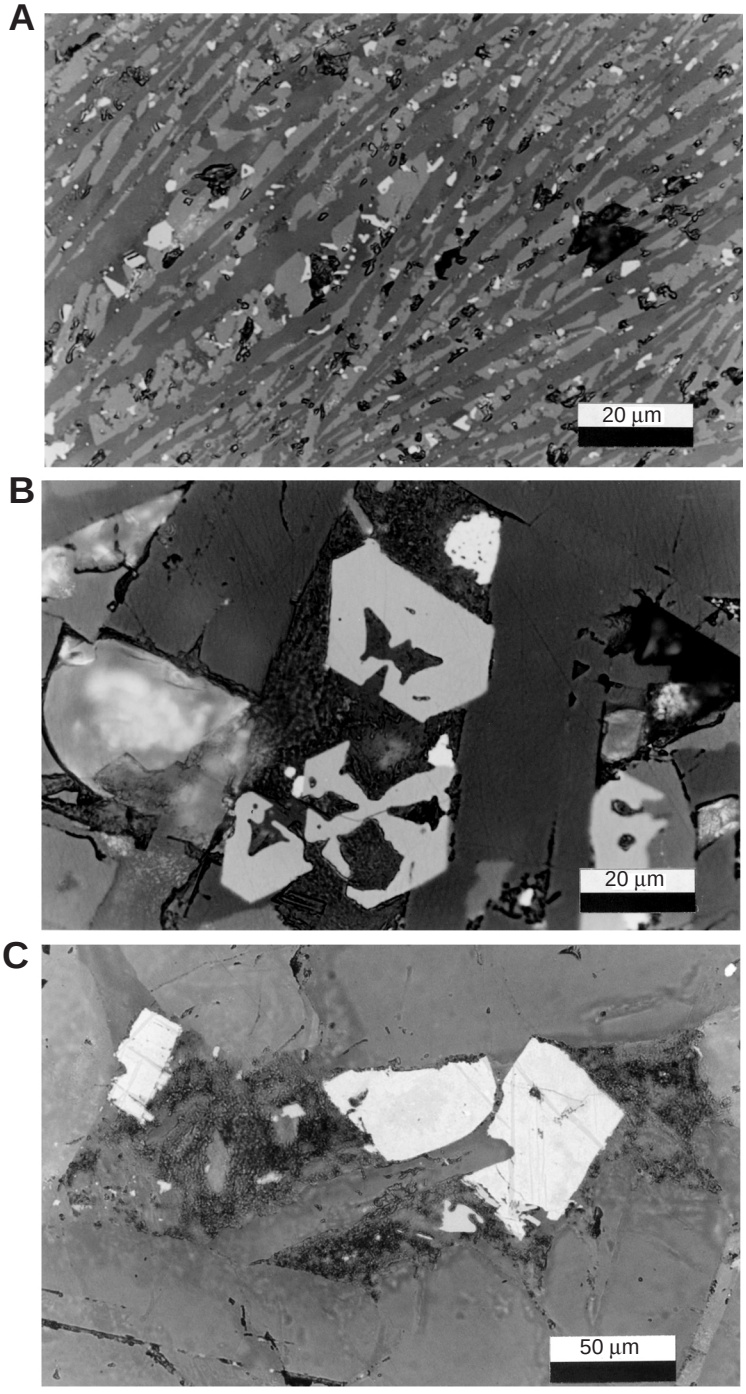

**Figure F10.** Scanning electron microscopic backscattered electron images showing features of the opaque minerals. **A.** Titanomagnetite pseudomorphs in pillow basalt show shrinkage curvature cracks. These cracks and their adjacent areas are filled or replaced by silicates as shown by the stains of darker contrast within the titanomagnetite pseudomorphs (Sample 187-1154A-8R-1, 135–140 cm [#20]). Scale bar = 1 µm. **B.** Submicroscopic Fe-Ti oxide mineral grains (gray-white dots) in interstitial glass (darkest area at central part of the two images) of pillow basalt (Sample 187-1159A-2R-1, 26–30 cm [#57]). The right image is an enlarged part of the central area of the left image. Three large subhedral to euhedral titanomagnetite pseudomorphs are a few micrometers across. Lath-shaped minerals are dark gray plagioclase and gray-white clinopyroxene. Scale bar = 5 µm.

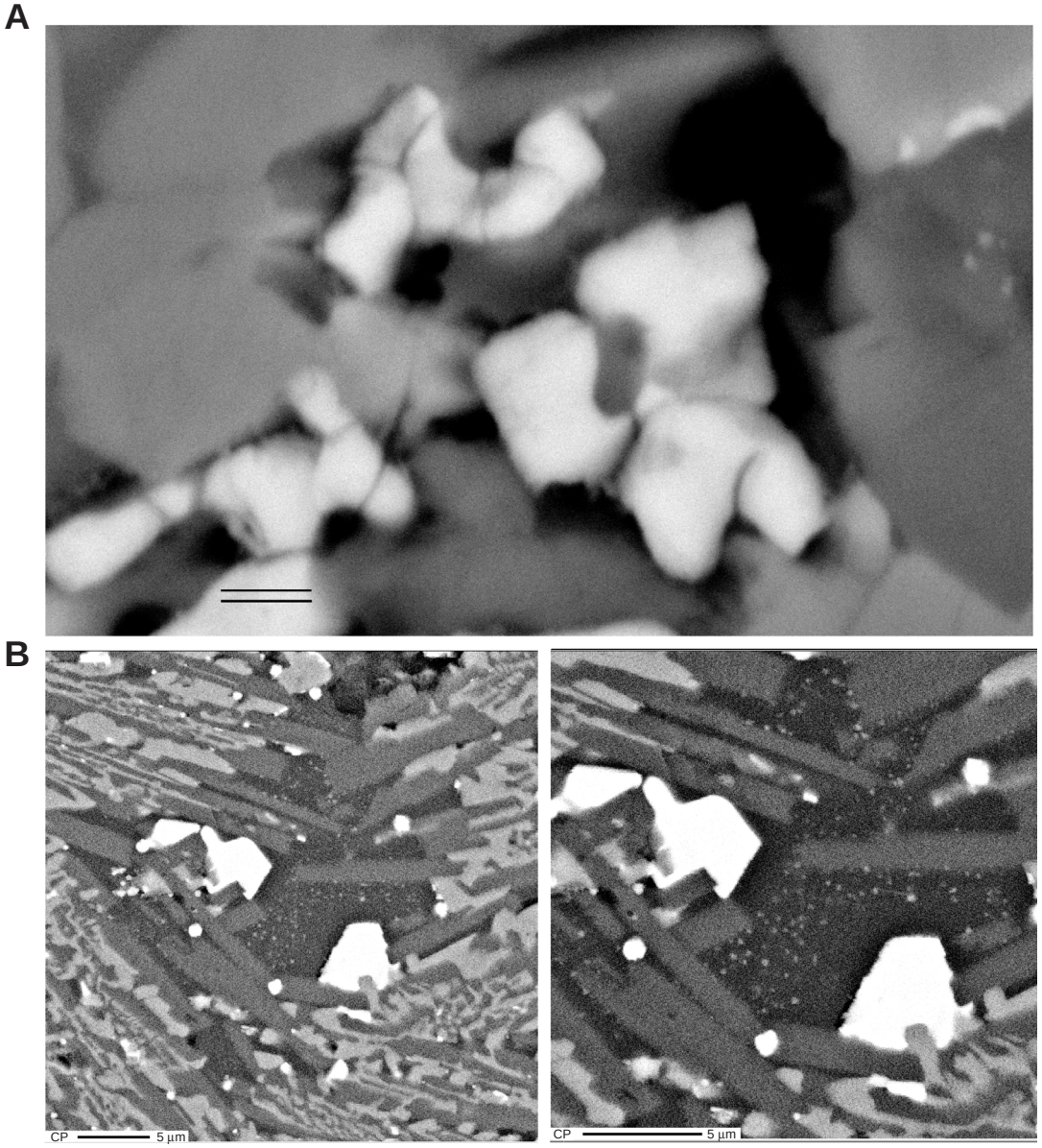

**Table T1.** Magnetic properties of the cored samples, Leg 187. (See **table notes.** Continued on next two pages.)

| Mantle province/ Sample number | Core, section, interval (cm) | Depth in basement (m) | NRM (A/m) | $k$ ($\times 10^{-3}$ SI) | $M_{rs}$ (A/m) | $M_s$ (A/m) | $M_{rs}/M_s$ | $B_c$ (mT) | $B_{cr}$ (mT) | $B_{cr}/B_c$ | $T_c$ (°C) |
|---|---|---|---|---|---|---|---|---|---|---|---|
| Transitional-Pacific | 187-1152A- | | | | | | | | | | |
| 1 | 1R-1, 15–20 | 0.15 | 3.36 | 2.69 | 321.5 | 609.7 | 0.527 | 35.8 | 49.8 | 1.391 | 282 |
| Transitional-Pacific | 187-1152B- | | | | | | | | | | |
| 2 | 2R-1, 53–61 | 0.53 | 0.53 | 2.01 | 254.6 | 378.0 | 0.674 | 64.8 | 84.3 | 1.301 | 318 |
| 3 | 3R-1, 11–17 | 5.31 | 0.48 | 1.90 | 207.3 | 418.9 | 0.495 | 37.0 | 63.4 | 1.714 | 348 |
| 4 | 4R-1, 63–69 | 13.83 | 1.84 | 1.76 | 168.8 | 270.0 | 0.625 | 57.6 | 75.9 | 1.318 | |
| 5 | 4R-2, 20–25 | 14.90 | 2.15 | 1.19 | 246.6 | 492.5 | 0.501 | 30.1 | 42.4 | 1.409 | 263 |
| 6 | 5R-1, 96–100 | 19.16 | 2.73 | 1.85 | 245.5 | 423.8 | 0.579 | 46.5 | 64.6 | 1.389 | |
| 7 | 5R-2, 11–17 | 19.81 | 1.08 | 1.62 | 95.2 | 177.5 | 0.536 | 57.9 | 89.7 | 1.549 | |
| 8 | 6R-1, 11–13 | 22.81 | 3.39 | 1.58 | 209.3 | 347.4 | 0.603 | 80.4 | 118.0 | 1.468 | |
| Pacific | 187-1153A- | | | | | | | | | | |
| 9 | 7R-4, 30–34 | 0.00 | 2.20 | 2.13 | 288.1 | 527.8 | 0.546 | 46.5 | 68.2 | 1.467 | |
| 10 | 8R-1, 48–52 | 0.48 | 6.10 | 1.43 | 284.7 | 436.7 | 0.652 | 47.9 | 58.4 | 1.219 | 288 |
| 11 | 8R-2, 33–39 | 1.79 | 8.12 | 1.47 | 309.8 | 570.4 | 0.543 | 44.6 | 64.4 | 1.444 | 257 |
| Pacific | 187-1154A- | | | | | | | | | | |
| 12 | 2R-1, 78–82 | 0.78 | 3.58 | 2.02 | 198.4 | 313.9 | 0.632 | 61.1 | 85.4 | 1.398 | |
| 13 | 3R-1, 80–85 | 4.80 | 2.94 | 1.95 | 336.0 | 474.8 | 0.708 | 87.8 | 107.0 | 1.219 | 255 |
| 14 | 3R-2, 32–37 | 5.77 | 1.20 | 2.24 | 351.1 | 490.9 | 0.715 | 86.8 | 108.0 | 1.244 | |
| 15 | 4R-1, 18–22 | 8.68 | 1.63 | 2.18 | 146.1 | 265.8 | 0.550 | 47.6 | 67.3 | 1.414 | |
| 16 | 4R-2, 77–80 | 10.71 | 1.50 | 2.10 | 193.9 | 306.8 | 0.632 | 56.6 | 73.1 | 1.292 | |
| 17C* | 5R-1, 85–89 | 14.35 | 0.44 | 1.78 | 181.1 | 326.2 | 0.555 | 48.4 | 67.2 | 1.388 | 329 |
| 17R* | 5R-1, 85–89 | 14.35 | 0.47 | 2.64 | 145.6 | 253.4 | 0.575 | 53.6 | 72.6 | 1.354 | 269 |
| 18C | 6R-1, 66–69 | 18.76 | 0.55 | 1.26 | 106.9 | 211.0 | 0.507 | 41.4 | 61.6 | 1.488 | |
| 18R | 6R-1, 66–69 | 18.76 | 0.81 | 2.59 | 256.1 | 467.8 | 0.547 | 32.4 | 43.7 | 1.349 | |
| 19C | 7R-1, 25–31 | 23.55 | 1.61 | 1.57 | 314.7 | 577.5 | 0.545 | 40.8 | 55.1 | 1.350 | |
| 19R | 7R-1, 25–31 | 23.55 | 1.38 | 2.08 | 191.9 | 289.9 | 0.662 | 65.3 | 80.5 | 1.233 | |
| 20C | 8R-1, 135–140 | 29.35 | 0.97 | 1.09 | 195.1 | 315.8 | 0.618 | 69.8 | 91.7 | 1.314 | 303 |
| 20R | 8R-1, 135–140 | 29.35 | 0.75 | 2.07 | 386.6 | 561.5 | 0.689 | 65.6 | 80.5 | 1.227 | 288 |
| 21C | 8R-2, 32–38 | 29.82 | 0.98 | 1.40 | 170.2 | 309.8 | 0.549 | 53.2 | 74.9 | 1.408 | |
| 21R | 8R-2, 32–38 | 29.82 | 0.41 | 2.25 | 288.5 | 456.1 | 0.633 | 49.4 | 61.1 | 1.237 | |
| 22 | 9R-1, 37–40 | 32.97 | 1.28 | 1.20 | 370.0 | 607.0 | 0.610 | 44.7 | 57.8 | 1.293 | |
| Transitional-Pacific | 187-1155A- | | | | | | | | | | |
| 23 | 4R-1, 18–22 | 7.18 | 5.72 | 1.22 | 542.3 | 838.1 | 0.647 | 59.4 | 73.5 | 1.237 | 281 |
| 24 | 7R-1, 55–59 | 21.75 | 9.76 | 2.19 | 372.4 | 908.4 | 0.410 | 14.8 | 18.3 | 1.236 | 229 |
| Transitional-Pacific | 187-1155B- | | | | | | | | | | |
| 25C | 2R-1, 45–53 | 0.45 | 2.65 | 1.06 | 236.5 | 372.8 | 0.635 | 59.0 | 74.0 | 1.254 | |
| 25R | 2R-1, 45–53 | 0.45 | 3.58 | 1.76 | 171.2 | 346.6 | 0.494 | 28.8 | 39.9 | 1.385 | |
| 26 | 3R-1, 58–62 | 4.18 | 1.96 | 1.82 | 63.9 | 129.5 | 0.493 | 30.5 | 45.5 | 1.492 | |
| 27 | 4R-2, 6–11 | 9.06 | 3.78 | 1.13 | 46.8 | 104.2 | 0.449 | 36.0 | 57.5 | 1.597 | |
| 28 | 5R-1, 99–102 | 13.19 | 0.84 | 0.89 | 89.4 | 157.6 | 0.567 | 78.9 | 133.0 | 1.686 | |
| 29 | 6R-3, 62–67 | 20.72 | 1.50 | 1.34 | 300.8 | 528.4 | 0.569 | 46.4 | 59.0 | 1.272 | |
| 30 | 7R-1, 125–130 | 23.05 | 6.29 | 1.80 | 123.2 | 304.0 | 0.405 | 39.6 | 71.0 | 1.793 | |
| 31 | 8R-1, 119–124 | 27.99 | 5.50 | 0.78 | 211.5 | 323.9 | 0.653 | 67.9 | 90.8 | 1.337 | 264 |
| 32 | 9R-1, 10–14 | 31.60 | 3.11 | 1.18 | 148.8 | 225.0 | 0.661 | 62.9 | 76.5 | 1.216 | |
| Indian | 187-1156A- | | | | | | | | | | |
| 33 | 2R-2, 67–72 | 2.17 | 5.35 | 1.21 | 184.6 | 352.5 | 0.524 | 49.9 | 79.7 | 1.597 | |
| 34 | 3R-1, 147–150 | 7.87 | 4.19 | 1.81 | 208.3 | 419.1 | 0.497 | 33.3 | 45.2 | 1.357 | |
| Indian | 187-1156B- | | | | | | | | | | |
| 35C | 2R-1, 73–77 | 0.73 | 1.06 | 1.03 | 233.7 | 547.2 | 0.427 | 31.7 | 54.0 | 1.703 | 346 |
| 35R | 2R-1, 73–77 | 0.73 | 6.85 | 1.58 | 184.4 | 337.8 | 0.546 | 46.1 | 67.6 | 1.466 | 260 |
| 36 | 3R-1, 2–6 | 5.82 | 7.67 | 1.41 | 210.0 | 547.3 | 0.384 | 23.4 | 36.3 | 1.551 | 307 |
| 37C | 4R-1, 26–30 | 15.46 | 9.98 | 1.29 | 291.7 | 474.2 | 0.615 | 52.1 | 64.5 | 1.238 | |
| 37R | 4R-1, 26–30 | 15.46 | 6.34 | 1.07 | 260.4 | 386.4 | 0.674 | 64.8 | 79.0 | 1.219 | |
| 38 | 4R-3, 38–41 | 18.16 | 3.68 | 1.50 | 349.0 | 606.4 | 0.575 | 33.3 | 41.0 | 1.231 | |
| 39 | 5R-1, 75–80 | 25.05 | 1.78 | 1.20 | 168.6 | 272.7 | 0.618 | 53.4 | 66.0 | 1.236 | |
| 40 | 6R-2, 64–70 | 30.74 | 3.40 | 0.76 | 155.5 | 259.1 | 0.600 | 65.8 | 93.2 | 1.416 | |
| Indian | 187-1157A- | | | | | | | | | | |
| 41 | 2R-1, 52–56 | 0.52 | 2.00 | 1.27 | 81.2 | 150.9 | 0.538 | 38.5 | 52.6 | 1.366 | 301 |
| 42 | 3R-1, 132–135 | 7.32 | 3.95 | 1.70 | 298.1 | 502.7 | 0.593 | 36.2 | 45.9 | 1.268 | |
| 43 | 4R-1, 32–37 | 15.72 | 5.40 | 1.16 | 228.6 | 348.9 | 0.655 | 58.8 | 73.0 | 1.241 | |

**Table T1 (continued).**

| Mantle province/ Sample number | Core, section, interval (cm) | Depth in basement (m) | NRM (A/m) | $k$ ($\times 10^{-3}$ SI) | $M_{rs}$ (A/m) | $M_s$ (A/m) | $M_{rs}/M_s$ | $B_c$ (mT) | $B_{cr}$ (mT) | $B_{cr}/B_c$ | $T_c$ (°C) |
|---|---|---|---|---|---|---|---|---|---|---|---|
| Indian | 187-1157B- | | | | | | | | | | |
| 44 | 2R-1, 65–69 | 0.65 | 3.23 | 1.46 | 208.5 | 399.1 | 0.522 | 38.6 | 53.9 | 1.396 | |
| 45 | 3R-1, 62–66 | 8.52 | 4.00 | 0.61 | 192.2 | 287.7 | 0.668 | 77.1 | 93.2 | 1.209 | |
| 46 | 4R-2, 42–46 | 14.33 | 5.07 | 1.49 | 301.6 | 456.6 | 0.660 | 60.0 | 73.1 | 1.218 | |
| 47 | 5R-2, 27–34 | 18.97 | 2.40 | 0.95 | 157.6 | 242.5 | 0.650 | 80.5 | 100.0 | 1.242 | |
| 48 | 6R-2, 143–148 | 24.53 | 3.91 | 1.35 | 149.3 | 290.0 | 0.515 | 49.4 | 86.0 | 1.741 | |
| 49 | 8R-1, 77–81 | 31.57 | 1.72 | 2.27 | 205.8 | 451.9 | 0.455 | 29.1 | 40.1 | 1.378 | |
| 50 | 9R-1, 10–14 | 35.90 | 2.53 | 1.44 | 200.7 | 347.6 | 0.577 | 55.3 | 82.9 | 1.499 | |
| Pacific | 187-1158A- | | | | | | | | | | |
| 51C | 2R-1, 15–20 | 0.15 | 5.42 | 1.10 | 284.1 | 471.1 | 0.603 | 64.7 | 87.3 | 1.349 | |
| 51R | 2R-1, 15–20 | 0.15 | 3.17 | 0.97 | 129.1 | 269.5 | 0.479 | 34.2 | 55.8 | 1.632 | |
| Pacific | 187-1158B- | | | | | | | | | | |
| 52 | 2R-1, 42–46 | 0.42 | 2.88 | 4.12 | 355.3 | 1040.2 | 0.342 | 14.6 | 19.9 | 1.363 | 270 |
| 53C | 3R-1, 1–6 | 5.61 | 1.93 | 5.33 | 234.6 | 634.0 | 0.370 | 16.4 | 21.0 | 1.280 | 443 |
| 53R | 3R-1, 1–6 | 5.61 | 4.85 | 4.09 | 268.1 | 768.1 | 0.349 | 14.6 | 20.9 | 1.432 | 377 |
| 54C | 4R-1, 34–37 | 10.94 | 9.35 | 1.61 | 255.7 | 404.8 | 0.632 | 68.1 | 83.4 | 1.225 | |
| 54R | 4R-1, 34–37 | 10.94 | 2.27 | 1.88 | 130.7 | 210.8 | 0.620 | 84.1 | 118.0 | 1.403 | |
| Pacific | 187-1158C- | | | | | | | | | | |
| 55 | 1W-1, 8–14 | 0.00 | 11.20 | 2.03 | 276.4 | 567.6 | 0.487 | 41.2 | 67.1 | 1.629 | |
| 56 | 2R-1, 134–137 | 1.34 | 3.21 | 4.14 | 291.3 | 835.3 | 0.349 | 15.7 | 21.6 | 1.376 | 326 |
| Pacific | 187-1159A- | | | | | | | | | | |
| 57C | 2R-1, 26–30 | 0.30 | 8.63 | 1.75 | 323.4 | 514.7 | 0.628 | 50.2 | 61.8 | 1.231 | |
| 57R | 2R-1, 26–30 | 0.30 | 6.48 | 1.62 | 224.2 | 331.2 | 0.677 | 70.4 | 88.1 | 1.251 | |
| 58 | 5R-1, 25–30 | 12.00 | 4.45 | 2.00 | 361.5 | 644.2 | 0.561 | 25.7 | 31.5 | 1.226 | |
| 59 | 6R-2, 1–5 | 17.50 | 7.68 | 2.05 | 298.8 | 457.3 | 0.653 | 41.4 | 47.9 | 1.157 | |
| 60 | 7R-2, 32–35 | 22.80 | 16.30 | 1.76 | 282.9 | 433.2 | 0.653 | 52.7 | 62.3 | 1.182 | 243 |
| Pacific | 187-1160A- | | | | | | | | | | |
| 61C | 2R-1, 23–25 | 0.23 | 0.90 | 0.61 | 112.8 | 176.4 | 0.639 | 81.1 | 103.0 | 1.270 | 319 |
| 61R | 2R-1, 23–25 | 0.23 | 0.64 | 1.07 | 115.7 | 237.1 | 0.488 | 38.0 | 53.4 | 1.405 | 293 |
| Pacific | 187-1160B- | | | | | | | | | | |
| 62 | 2R-1, 19–25 | 0.19 | 1.43 | 1.56 | 159.0 | 279.3 | 0.569 | 29.3 | 35.4 | 1.208 | |
| 63 | 4R-1, 72–77 | 10.12 | 9.29 | 24.00 | 122.1 | 1249.0 | 0.098 | 3.6 | 9.9 | 2.725 | 177 |
| 64 | 6R-2, 129–133 | 21.59 | 2.55 | 1.25 | 107.6 | 217.6 | 0.495 | 27.0 | 36.1 | 1.337 | |
| 65 | 7R-1, 59–62 | 28.49 | 1.89 | 22.55 | 166.7 | 1487.2 | 0.112 | 4.8 | 12.0 | 2.510 | 172 |
| 66C | 8R-1, 30–36 | 33.90 | 0.30 | 2.20 | 142.2 | 327.8 | 0.434 | 30.2 | 46.7 | 1.546 | |
| 66R | 8R-1, 30–36 | 33.90 | 0.39 | 2.68 | 59.7 | 151.9 | 0.393 | 25.4 | 40.9 | 1.610 | |
| 67 | 9R-1, 111–116 | 38.21 | 4.10 | 14.82 | 204.0 | 1550.7 | 0.132 | 6.4 | 14.9 | 2.328 | 231 |
| Indian | 187-1161A- | | | | | | | | | | |
| 68 | 1W-CC, 21–25 | 0.00 | 0.33 | 1.65 | 151.0 | 345.7 | 0.437 | 29.2 | 47.8 | 1.637 | |
| 69C | 3R-1, 121–124 | 5.21 | 0.34 | 1.26 | 130.4 | 247.2 | 0.528 | 44.3 | 60.3 | 1.361 | |
| 69R | 3R-1, 121–124 | 5.21 | 0.83 | 1.38 | 249.4 | 449.3 | 0.555 | 35.6 | 45.6 | 1.281 | |
| 70C | 4R-1, 49–53 | 13.89 | 4.78 | 1.33 | 261.8 | 410.9 | 0.637 | 54.1 | 67.9 | 1.255 | 253 |
| 70R | 4R-1, 49–53 | 13.89 | 1.00 | 1.81 | 166.8 | 336.5 | 0.495 | 24.6 | 33.6 | 1.366 | 298 |
| 71 | 5R-1, 35–39 | 23.15 | 3.16 | 2.09 | 163.5 | 378.3 | 0.432 | 22.8 | 33.2 | 1.456 | |
| Indian | 187-1161B- | | | | | | | | | | |
| 72 | 1W-1, 65–69 | 0.00 | 2.89 | 4.90 | 297.1 | 984.1 | 0.302 | 11.3 | 15.7 | 1.389 | 281 |
| 73 | 2R-1, 19–23 | 0.19 | 0.37 | 1.87 | 166.6 | 382.9 | 0.435 | 25.1 | 36.4 | 1.450 | |
| Pacific | 187-1162A- | | | | | | | | | | |
| 74 | 5R-1, 33–37 | 22.33 | 0.12 | 2.34 | 98.5 | 356.5 | 0.276 | 29.0 | 82.9 | 2.859 | 367, 580 |
| Pacific | 187-1162B- | | | | | | | | | | |
| 75-1 | 5R-1, 81–86 | 17.21 | 0.41 | 1.25 | 89.9 | 177.9 | 0.506 | 25.6 | 34.5 | 1.348 | 384 |
| 75-2 | 5R-1, 81–86 | 17.21 | 1.55 | 2.44. | 84.1 | 161.3 | 0.522 | 24.4 | 35.0 | 1.434 | 405 |
| 75-3 | 5R-1, 81–86 | 17.21 | 0.24 | 1.57 | 69.6 | 151.5 | 0.460 | 25.6 | 35.7 | 1.395 | 369 |
| Transitional-Pacific | 187-1163A- | | | | | | | | | | |
| 76 | 2R-1, 135–140 | 1.35 | 1.60 | 1.02 | 138.0 | 293.8 | 0.470 | 38.2 | 61.0 | 1.597 | 288 |
| 77 | 3R-2, 28–33 | 6.13 | 4.45 | 1.00 | 163.6 | 260.2 | 0.629 | 56.1 | 70.2 | 1.251 | |
| 78 | 4R-1, 113–117 | 11.53 | 4.88 | 0.88 | 153.6 | 250.8 | 0.613 | 63.1 | 80.8 | 1.281 | 301 |
| 79 | 5R-2, 23–28 | 16.45 | 6.79 | 0.96 | 216.2 | 765.8 | 0.282 | 55.5 | 65.7 | 1.184 | 270 |
| 80 | 6R-2, 70–75 | 21.67 | 2.85 | 1.30 | 203.7 | 320.3 | 0.636 | 51.8 | 66.3 | 1.280 | |
| 81 | 7R-2, 49–55 | 26.01 | 5.32 | 0.98 | 146.9 | 233.5 | 0.629 | 66.9 | 81.1 | 1.212 | |
| 82 | 9R-1, 25–28 | 33.35 | 4.75 | 0.91 | 196.5 | 306.5 | 0.641 | 70.0 | 85.9 | 1.227 | |
| 83 | 10R-1, 47–52 | 38.57 | 5.06 | 1.04 | 191.6 | 318.6 | 0.601 | 50.9 | 62.8 | 1.234 | |
| 84 | 11R-1, 58–63 | 42.68 | 2.42 | 1.06 | 246.7 | 427.0 | 0.578 | 49.3 | 65.6 | 1.331 | |

**Table T1 (continued).**

| Mantle province/ Sample number | Core, section, interval (cm) | Depth in basement (m) | NRM (A/m) | $k$ ($\times 10^{-3}$ SI) | $M_{rs}$ (A/m) | $M_s$ (A/m) | $M_{rs}/M_s$ | $B_c$ (mT) | $B_{cr}$ (mT) | $B_{cr}/B_c$ | $T_c$ (°C) |
|---|---|---|---|---|---|---|---|---|---|---|---|
| Transitional-Pacific | 187-1164A- | | | | | | | | | | |
| 85C | 3R-1, 34–38 | 3.94 | 1.01 | 1.46 | 2.3 | 61.9 | 0.037 | 12.2 | 68.2 | 5.590 | 260 |
| 85R | 3R-1, 34–38 | 3.94 | 1.14 | 1.22 | 290.2 | 458.7 | 0.633 | 46.4 | 54.5 | 1.175 | 253 |
| 86C | 4R-1, 7–11 | 8.27 | 1.09 | 0.99 | 196.6 | 343.3 | 0.573 | 58.4 | 75.6 | 1.295 | |
| 86R | 4R-1, 7–11 | 8.27 | 1.40 | 1.39 | 197.7 | 309.5 | 0.639 | 66.4 | 83.8 | 1.262 | |
| Transitional-Pacific | 187-1164B- | | | | | | | | | | |
| 87 | 2R-1, 0–7 | 0.00 | 2.49 | 1.60 | 226.1 | 504.0 | 0.449 | 26.1 | 36.3 | 1.391 | |
| 88 | 3R-1, 69–72 | 6.09 | 3.05 | 1.02 | 243.9 | 393.6 | 0.620 | 37.6 | 45.8 | 1.218 | |
| 89 | 4R-1, 53–59 | 10.93 | 3.93 | 1.17 | 176.8 | 307.7 | 0.575 | 43.5 | 57.4 | 1.320 | |
| 90 | 5R-1, 64–67 | 20.44 | 5.42 | 0.83 | 117.8 | 248.8 | 0.474 | 37.4 | 54.9 | 1.468 | 248 |
| 91 | 6R-1, 15–20 | 24.35 | 2.97 | 1.12 | 118.7 | 201.3 | 0.590 | 53.8 | 76.4 | 1.420 | |
| 92 | 7R-1, 101–106 | 29.91 | 2.78 | 0.74 | 130.6 | 217.4 | 0.601 | 58.1 | 87.7 | 1.509 | |
| 93 | 9R-1, 105–109 | 48.15 | 3.11 | 1.12 | 146.3 | 225.0 | 0.650 | 75.6 | 99.2 | 1.312 | 279 |
| 94 | 10R-1, 8–15 | 56.48 | 4.88 | 0.98 | 134.2 | 228.4 | 0.587 | 60.1 | 90.8 | 1.511 | 262 |

Notes: * = paired samples from the core zone (C) and rim zone (R) of pillows. $k$ = magnetic susceptibility (volume specific), $M_{rs}$ = remanent saturation magnetization, $M_s$ = saturation magnetization, $B_c$ = coercivity, $B_{cr}$ = remanent coercivity, $T_c$ = Curie temperature (in air). Mantle province and sample depth data are from Shipboard Scientific Party (2001).

**Table T2.** Summary of magnetic properties of the three rock types.

| Magnetic Property | Pillow basalts | Massive basalts | Metadiabase |
|---|---|---|---|
| Alteration or metamorphism | Slightly or pervasively altered, low-temperature oxidation | Nearly unaltered | Highly altered, greenschist facies metamorphism |
| Wasp-waisted hysteresis loops | Yes | No | No |
| Grain size (magnetic domain) | SSD to PSD | Larger PSD | Larger PSD |
| Curie temperature | 250°–400°C | 170°–230°C | ~370° and 580°C |
| Thermomagnetic curve | Irreversible | Almost reversible (in vacuum) | Irreversible |
| Thermal demagnetization of low-*T* IRM | — | Transition at ~55 K | Transition at ~120 K (Verwey transition) |
| Magnetic minerals | Titanomaghemite | Titanomagnetite | Magnetite + maghemite(?) |

Note: PSD = pseudosingle domain, SSD = stable single domain.